2004

Adhesion of copper to Teflon® FEP and PFA surfaces modified by vacuum UV photo-oxidation downstream from Ar microwave plasma

Wagner Dasilva

Adhesion of Copper to Teflon® FEP and PFA Surfaces Modified by Vacuum UV Photo-oxidation Downstream from Ar Microwave Plasma

Wagner Dasilva

September, 2004

SUBMITTED IN PARTIAL FULFILLMENT OF THE REQUIREMENTS FOR THE DEGREE OF MASTER OF SCIENCE

APPROVED:

G. A. Takacs

Project Advisor, Dr. Gerald Takacs

T. C. Morrill

Chemistry Department Head
Dr. Terence Morrill

Adhesion of Copper to Teflon® FEP and PFA Surfaces Modified by Vacuum UV Photo-oxidation Downstream from Ar Microwave Plasma

September, 2004

Abstract- Poly(tetrafluoroethylene-co-hexafluoropropylene) (FEP) and tetrafluoroethylene-co-perfluoroalkoxy vinyl ether) (PFA) surfaces were exposed to vacuum UV (VUV) photo-oxidation downstream from Ar microwave plasma. The modified surfaces showed the following: (1) an improvement in wettability as observed by water contact angle measurements; (2) surface roughening; (3) defluorination of the surface; and (4) incorporation of oxygen as CF-O-CF_2, CF_2-O-CF_2 and CF-O-CF_3 moieties for FEP and CF-O-CF_2, CF_2-O-CF_2 and CF-O-C_nF_{2n+1} moieties for PFA. With long treatment times, cohesive failure of copper sputter-coated onto the modified surface occurred within the modified FEP and PFA and not at the Cu-FEP and Cu-PFA interface.

List of Figures

List of Tables

Acknowledgements

I would like to first thank God for the guidance and insights and all my family members, whose names will not fit on this page, for their total support.

I specially would like to thank Dr. Gerald Takacs, my advisor and friend, for the guidance, insights and mentoring in the professional and personal life. I want to thank my research team for all the help Dr Alan Entenberg, Dr Bruce Kahn both at RIT and Dr Thomas Debies at Xerox Corporation, I also want to thank Dr. Rosenberg and Dr. Miri for being in my oral committee.

I would like to thank Dr. Terence Morrill for his help and support and his believe in my skills as a student and professional.

I really appreciate all the help from the RIT staff, especially Brenda Mastrangelo, Denise Lake, Tom Allston, all the stock room staff, human resources, co-op and career office, and Interfaith Center.

I also appreciate all the help and cooperation from my labmates and student group.

Finally I want to thank all the RIT-Mini Baja team, especially Jason Rounds for all the support and friendship. Last, but not least, I want to thank all my friends around the world, whose names again wouldn't fit on this single page.

Thank you all very much for all the support and for being there for me when I most needed it.

Table of Contents

1. INTRODUCTION

Fluoropolymers, like poly(tetrafluoroethylene) (PTFE), poly(tetrafluoroethylene-co-hexafluoropropylene) (FEP) and PFA (polytetrafluoroethylene-co-perfluoroalkoxy vinyl ether) have been extensively used in space applications, protective coatings, microelectronics packaging and biotechnology. However, their low surface energy properties present considerable challenges for adhesion and wettability when bonding to other materials, such as the conductor copper. Therefore, processes, that provide surface modification of these materials, are of considerable interest [1].

Methods, that have been employed for modification of the semi-crystalline thermoplastics FEP and PFA, to improve adhesion with Cu include:

(1) wet chemical pre-treatment with sodium naphthalenide [2-4];

(2) UV laser photolysis at 248 and 266 nm of tetramethyl ammonium hydroxide solution [5];

(3) treatment in radio-frequency (RF) plasmas containing Ar, He, O_2 and H_2 followed by a silane coupling agent [6];

(4) treatment in radio-frequency (RF) Ar plasma followed by reaction with air to form surface peroxides and hydroperoxides for subsequent UV-induced graft co-polymerization [7, 8];

(5) irradiation with x-ray [9] and e-beams [2, 3];

(6) exposure to remote RF plasmas [10-12].

(7) treatment in gaseous microwave (MW) plasma mixtures of N_2, O_2 and H_2 [13, 14]; and

(8) high temperature lamination at 380°C [15].

Recently, the adhesion of copper was enhanced with treatment of PTFE surfaces downstream from two sources of vacuum UV (VUV) radiation: (1) a unique high-pressure windowless helium source that was designed to produce a continuum of excimer (He_2*)

radiation from 58-110 nm [16] and (2) a windowless low-pressure microwave (MW) discharge of He or Ar which is primarily a VUV line source due to emission from excited rare gas atoms [17].

Surface modification of PFA with vacuum UV (VUV) radiation downstream from a helium MW plasma have been reported to induce defluorination, improve wettability, and incorporate oxygen upon exposure to air. Laser-assisted Fourier transform mass spectrometry on the VUV-treated PFA samples resulted in a series of high molecular weight fragments that indicated crosslinking at the surface [18].

Reports in the literature on the effects of UV and VUV irradiation of polymers to control the adhesion of Cu are sparse [16,17,19]. Egitto et al. [20] measured practical adhesion of sputtered chromium films to Kapton-H polyimide (PI) treated downstream from an oxygen microwave (MW) plasma (devoid of ion bombardment) and in a DC-glow discharge (in the presence of ion bombardment) using 90° peel tests. Kapton is a registered trademark of E.I. du Pont de Nemours & Co., Wilmington, DE and is a formulation produced by curing a poly(amic acid), whose precursors are pyromellitic dianhydride (PMDA) and oxydianiline (ODA). Downstream-plasma treatment reduced practical adhesion levels for Kapton-H PI, while treatment in the DC glow produced adhesion about triple the value measured for untreated films. These adhesion results were attributed to the difference in degree of ion bombardment in the various plasma conditions and the concomitant difference in the relative amount of chain scission and cross-linking reactions. Rozovskis et al. [21] conducted oxygen reactive ion etching of PI and observed a correlation between enhancement of Cu peel strength and content

of oxygen-containing groups at PI surface. Their conclusions confirmed the idea of competing rates for strengthening (cross-linking) and weakening (bond scission) effects associated with formation of a weak boundary layer (WBL). When PI is exposed to UV radiation, good adhesion of Cu to the modified surface is observed at short treatment times, while at long treatment times, cohesive failure occurred within the modified polymer and not at the Cu-polymer interface [19].

In the present thesis, the adhesion of Cu was investigated on FEP and PFA surfaces that were modified with 104.8 and 106.7 nm VUV radiation downstream from low-pressure Ar MW plasma. During most of the experiments, oxygen flowed over the VUV-exposed substrates.

2. EXPERIMENTAL

2.1 Materials

Commercially available films of the random co-polymer Teflon® FEP [–(CF_2-CF_2)$_x$-(CF_2-$CF(CF_3)$–]$_n$ where x ≅7 and Teflon® PFA [–(CF_2-CF_2)$_n$-(CF_2-$CFOC_3F_7$)$_m$–] (n/m= 39), with thicknesses of 50.8 μm were obtained from American Durafilm, Holliston, MA. For most of the experiments, the following effective cleaning procedure, involving treatment in ultrasonic baths of first methanol and then acetone at room temperature for 5 min followed by over-night drying in air at room temperature [18] or in a vacuum oven for 4 h at 90 – 100 °C, was employed. For PFA before attempting modification of the surface, a variety of cleaning procedures to remove potential contamination from lubricants used in the thermal mechanical processes to form the polymer mass into commercial film were evaluated by X-ray Photoelectron Spectroscopy (XPS). Some experiments were also carried out using hexane as the solvent, since it often is used in surface analysis research to remove any silicone oil or grease due to contamination from processing samples in a low vacuum system. The cleaned PFA and FEP films were placed in the vacuum chamber (Fig. 1) and mounted under an aluminum ring with an area of 3.8 cm^2 exposed to the VUV radiation.

® Teflon is a registered trademark of E. I. duPont de Nemours & Co., Wilmington, DE.

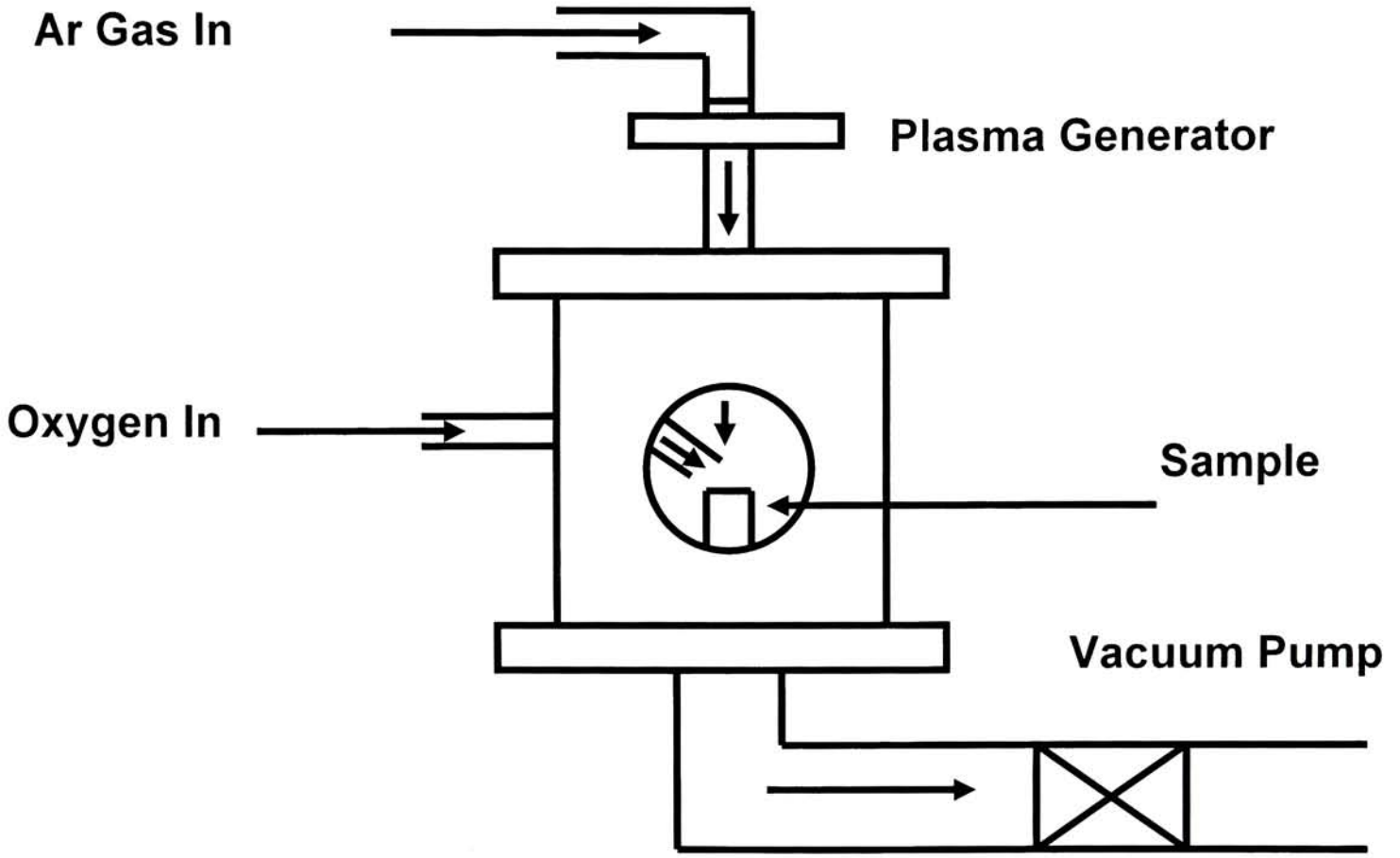

Figure 1. Schematic diagram of a microwave plasma apparatus

2.2 Radiation source

Low-pressure argon MW plasma, operating at a frequency of 2.45 GHz (with the difference between the forward and reflected power being 60 W) was used to modify the surface of FEP and PFA located downstream from the plasma.

The apparatus was similar to that used in the studies of etching, fluorination and defluorination of polyimide downstream from O_2-CF_4-Ar microwave plasma [21-26] except that in the present study the emission from the Ar discharge was aligned to maximize the interaction of photons with the substrate (Fig. 1). Oxygen was introduced into the vacuum system about 3 cm above the sample. The flow rates for both argon and oxygen were either 20 or 50 sccm. In one series of experiments, the Ar flow rate was maintained at 20 sccm and the oxygen flow rate was varied from 0-20 sccm. The reaction chamber pressure was maintained in the range (2.7 -5.3) x 10^1 Pa. The samples were placed 23.8 cm downstream from the discharge. At this distance, deactivation and recombination processes involving charged particles and metastables, which occur via homogeneous and heterogeneous collisions in transit to the substrate, make their contribution negligible and thus the interaction of VUV photons with the substrate is maximized [27, 28].

The low-pressure MW discharge produces radiation that is primarily a line source due to emission from excited Ar atoms, as shown in equation (1).

$$Ar^* = Ar + h\nu \qquad (1)$$

Neutral atomic resonance lines, arising from $^3P_1 \rightarrow {}^1S_0$ and $^3P_2 \rightarrow {}^1S_0$ transitions, occur at 104.8 and 106.7 nm for Ar, respectively [29]. For microwave excitation, emission continua from the rare gas excimer (Ar_2^*), that are formed by the pressure-sensitive reaction (2), have only been observed at pressures above 1.7×10^4 Pa [30].

$$Ar^* + Ar + M = Ar_2^* + M \qquad (2)$$

2.3 Contact angle measurements

Advancing contact angles [17] for 5µl DI water droplets were measured at 25°C in air before and after treatment with a Rame-Hart, Inc. goniometer model 100-00 using the sessile drop method. The accuracy of contact angle measurements was ±3°.

2.4 X-ray photoelectron spectroscopy

The samples were analyzed ex-situ after modification with X-ray Photoelectron Spectroscopy (XPS), a surface analysis technique that provides elemental, chemical state and quantitative analyses for the top 2 – 5 nm of a sample's surface. A Physical Electronics Model 5800 XPS system was employed for the characterization. A region about 800 µm in diameter was analyzed. The FEP and PFA films were prepared by cutting sections from the sample and mounting them beneath a molybdenum sample mask for exposing to the X-ray beam. The atomic percentages reported for carbon and fluorine are precise to within 2%,

while the At% for oxygen is within 20%. The uncertainties translate to about 0.07 units in the F/C ratio. The samples were irradiated with monochromatized Al Kα radiation (1486 eV) and charge neutralized with a flood of low energy electrons from a BaO field emission charge neutralizer. This method of analysis minimized radiation damage to the samples. High-resolution XPS spectra in the C 1s and O 1s regions were used to determine the chemical environment changes resulting from modification by VUV exposure. The analysis was performed at an angle of 45° between the sample and analyzer. The spectra were curve fitted using the software package provided by the instrument's supplier. The software utilizes commercial Matlab© routines for data processing.

2.5 Metallization

A DC planar magnetron [17] (manufactured by US Inc., Campbell, CA) was used to deposit about 300 nm of sputtered copper film. The film thickness and deposition rate were read on a quartz crystal rate deposition monitor. Research grade argon (99.997% pure) was introduced through a mass flow controller. The copper targets (50 mm diameter and 5 mm thick) were 99.9% pure. After the sputtering plasma was ignited, the target was pre-sputtered, while a shutter covered the substrate for about 2 min to allow the plasma to reach steady state during the establishment of the pressure and deposition rate.

The typical discharge voltage, current, and power were about 500 V, 0.500 A, and 250 W, respectively. There was a fixed argon working gas pressure of 0.3 Pa and fixed deposition rate of about 0.30 nm/s. The base pressure in the high vacuum chamber was less than 4.0 x 10^{-3} Pa. However, the effective base pressure during sputtering was closer to about 1.3 x 10^{-2} Pa because the diffusion pump was throttled.

2.6 Adhesion testing

Scotch Brand 3M tapes were used to check the adhesion of the copper film. The following 48 mm wide high-strength packaging tapes were used: #3750-G, #3650-C (Super Clear Tape), and #3501. The tape was slowly (~2 cm/s) peeled by hand from the copper film. During the peel test, Scotch Duct Tape (or its equivalent) was used to keep the film-substrate flat. After the tape test, the percentage of copper remaining on the substrate surface was estimated visually and defined as the "% adhesion." For intermediate adhesion values (from 20 to 80%), the absolute uncertainty was estimated to be $\pm$ 10%. In cases of very good adhesion, e.g. 97 $\pm$ 2 %, very poor adhesion, e.g. 4 $\pm$ 2 %, the absolute uncertainty becomes correspondingly lower and is estimated to be about $\pm$ 2%. For a comparison of relative adhesion strengths of various tapes to steel, see ref. [31].

2.7 SEM imaging

A Hitachi S-4500 field emission SEM was used to analyze the surface morphology of the photo-oxidized FEP and PFA films. The treated and untreated samples were placed onto

carbon adhesive tabs on Al stubs and coated with a thin conductive Au film of ca. 20 nm thickness.

3.0 RESULTS

3.1 Photo-etching rate

Negligible weight loss was observed for FEP indicating photo-etching rates of ≤ 1 nm/min, as show below , different than PTFE [17].

Table 1: Results of Photo-etching rate for FEP.

Initial Weight	Final Weight	Weight Gain	Weight Loss	Calculated Etch Rate
0.33020g	0.33030g	0.0001	-	-0.99 nm/min
0.34330g	0.34320g	-	0.0001	+0.99 nm/min

Photo etching rate is calculated by:

Photo-etching rate = thickness loss/time of treatment = weight loss/ density x area/treatment time

Where:
Density = 2.15 g/cc [32]
Area = 3.88 cm^2
Treatment time = 120 minutes

3.2 Water contact angle results

For FEP treated with VUV and oxygen flowing over the surface, the water contact angle showed an increase in hydrophilicity (decrease in contact angle) with exposure time from untreated FEP (105^o) to a minimum saturation value (ca. 76^o) suggesting that an equilibrium surface composition was established (Fig. 2).

While for PFA treated with VUV and oxygen flowing over the surface, the water contact angle showed an increase in hydrophilicity with exposure time from untreated PFA (110^{o}) to a minimum value of ca. 70^{o} (Fig. 3).

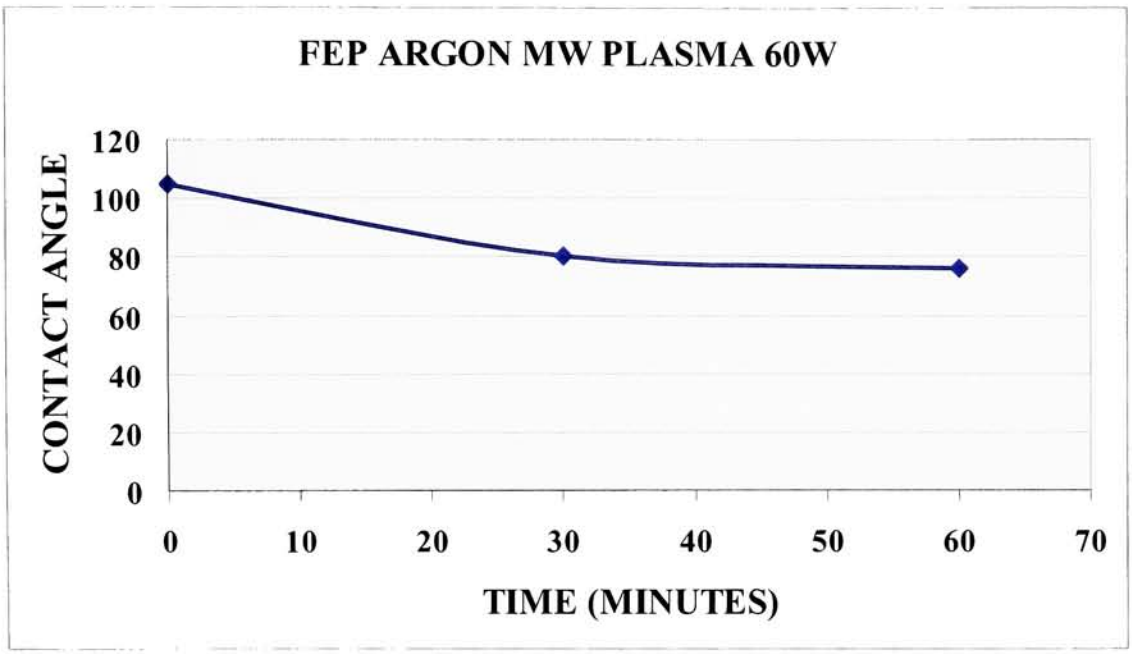

Fig. 2. Water contact angle for FEP as a function of treatment time for Ar MW plasma with oxygen flowing over the surface. Flow rates for both Ar and oxygen are 20 sccm.

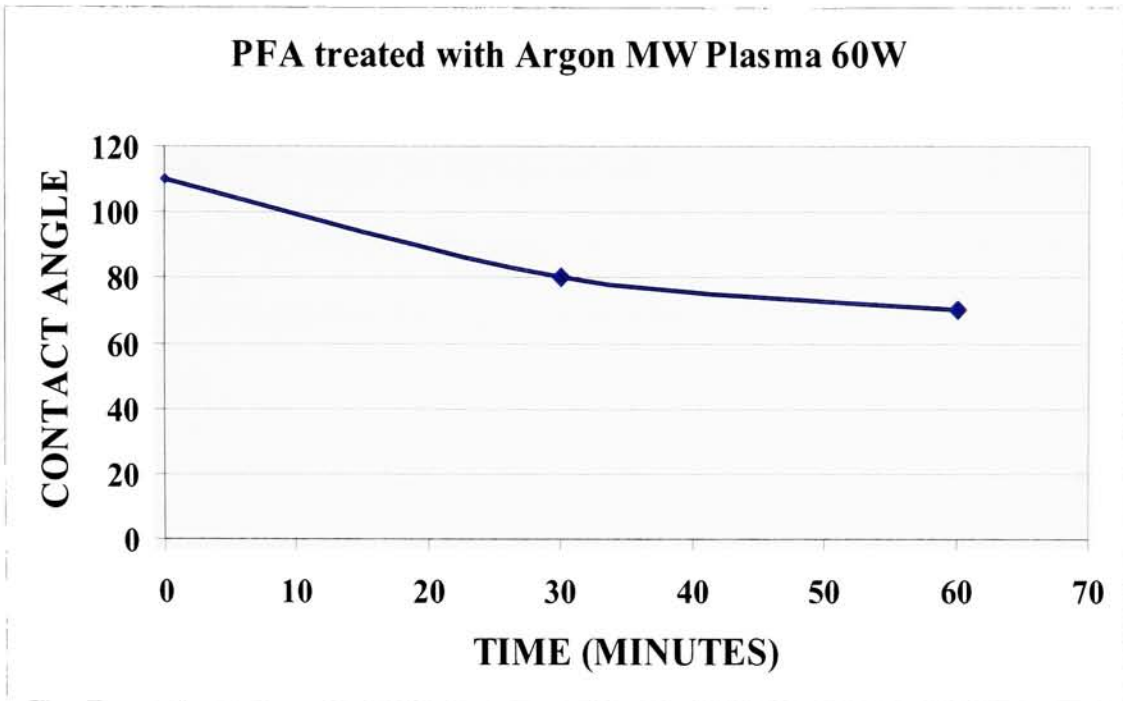

Fig. 3. Water contact angle for PFA as a function of treatment time for Ar MW plasma with oxygen flowing over the surface. Flow rates for both Ar and oxygen are 20 sccm.

3.3 SEM results

Figures 4(a) and (b) compare the SEM micrographs for untreated FEP and FEP treated using 20 sccm Ar and 20 sccm of oxygen flowing over the surface of the substrate. Change in surface roughness was observed at magnifications of 35 kX, bar size 857nm.

Figures 5 (a) and (b) compare the SEM micrographs for untreated PFA and PFA treated also using 20 sccm Ar and 20 sccm of oxygen flowing over the surface of the substrate. Change in surface morphology was also observed upon treatment using magnification and bar size as above.

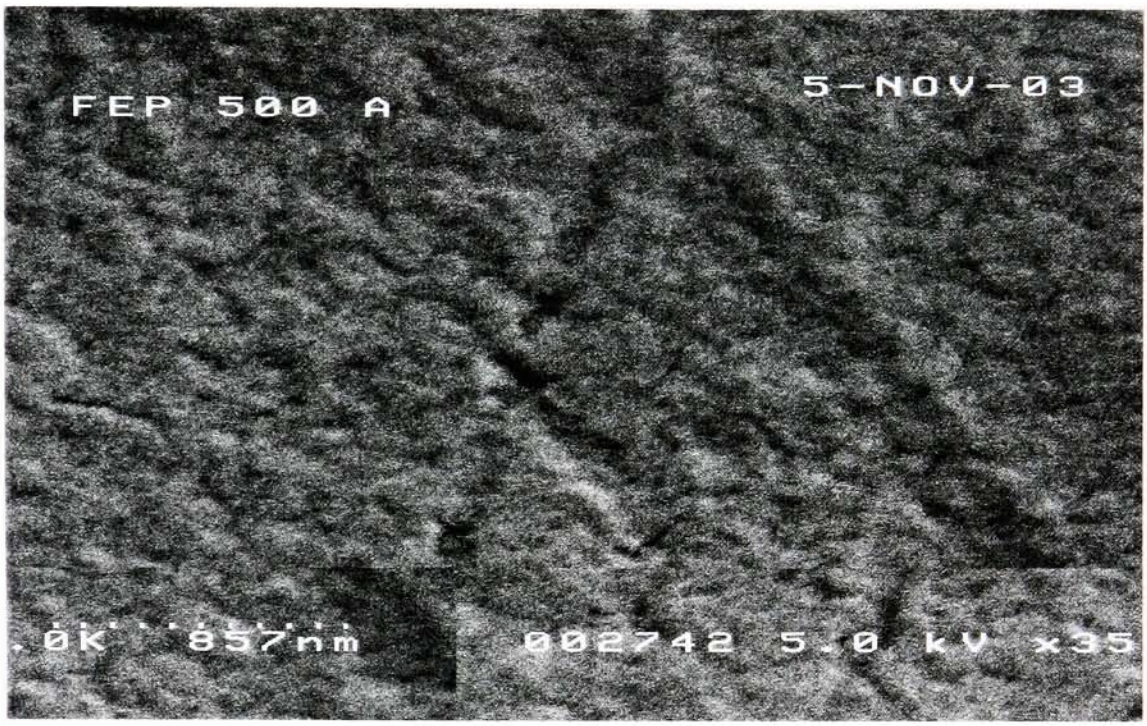

Fig. 4(a) SEM micrographs of untreated FEP

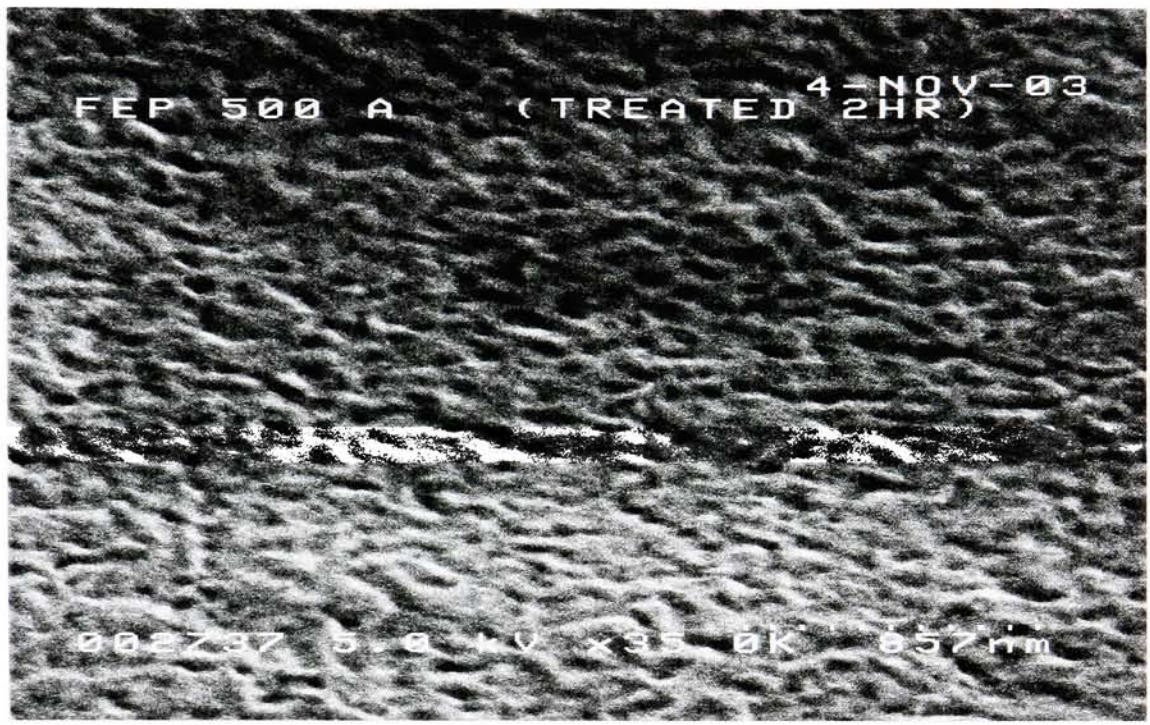

Fig. 4(b) FEP treated for 2 hr downstream from Ar MW plasma with flow rates of 20 sccm for both Ar and oxygen.

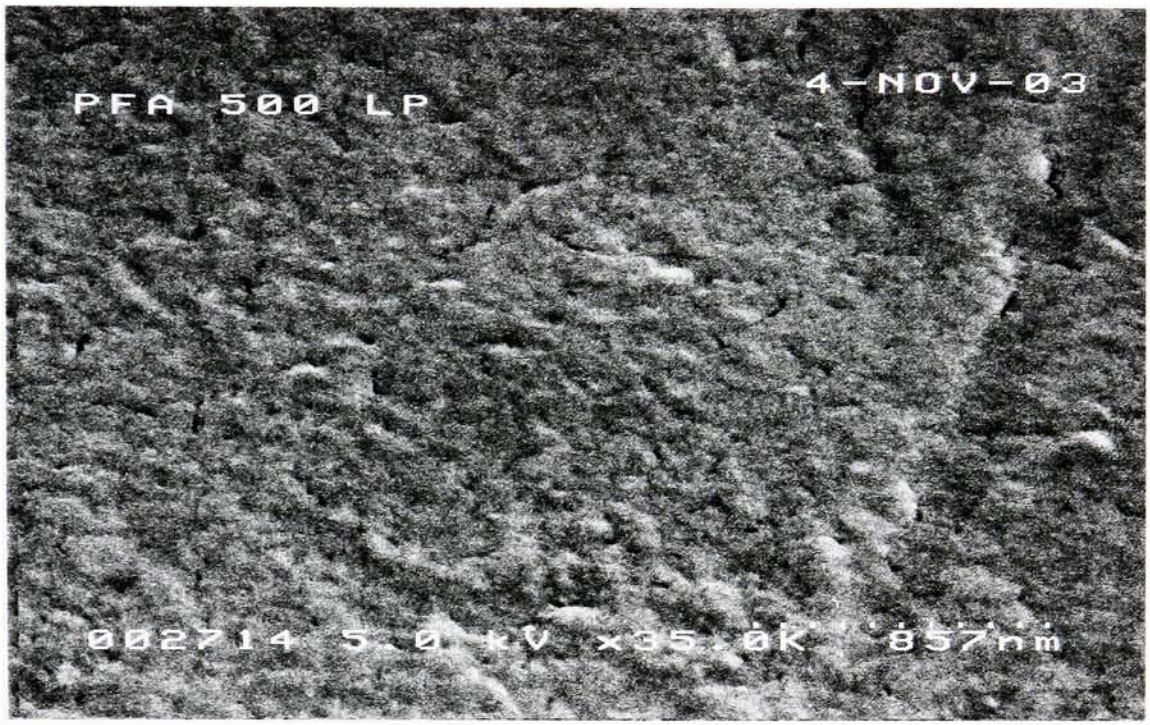

Fig. 5(a). SEM micrographs of untreated PFA

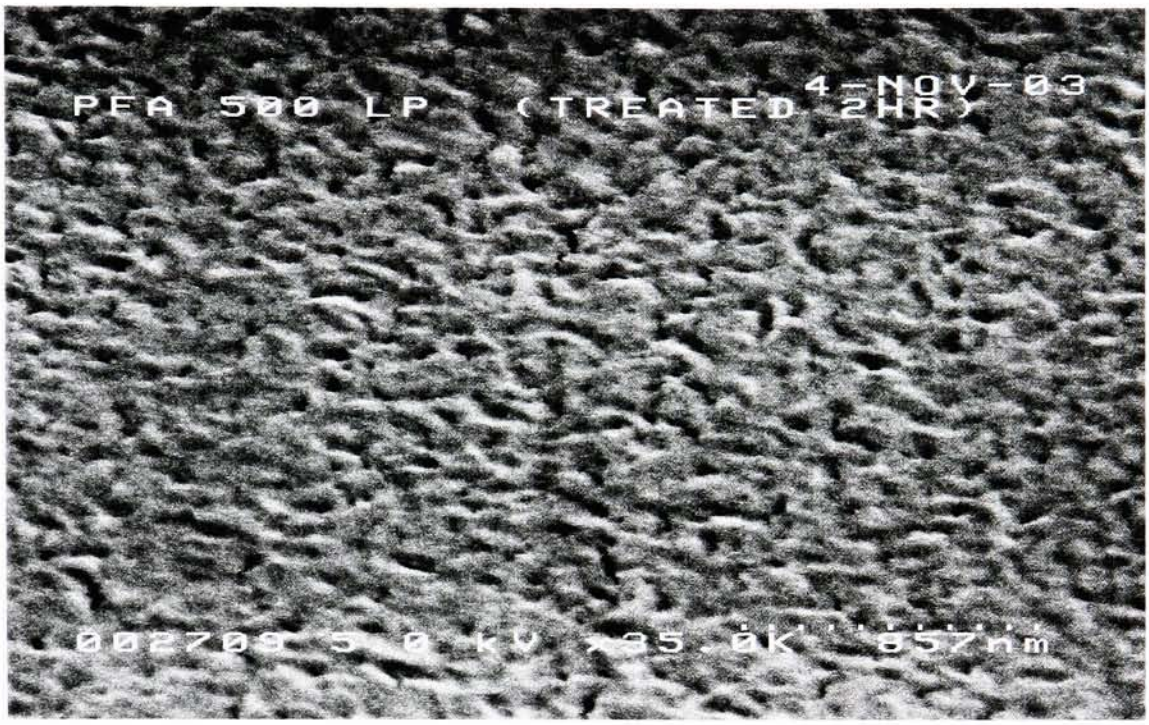

Fig. 5(b) PFA treated for 2 hr downstream from Ar MW plasma with flow rates of 20 sccm for both Ar and oxygen.

3.4 Cu Adhesion results

The percentage of Cu remaining on the modified FEP and PFA surfaces using flow rates of 20 and 50 sccm are reported as % adhesion and plotted as a function of treatment time in Figs. 6-9. At short treatment times, there is good adhesion of Cu to the modified surface. While at long treatment times greater than 1h, all of the Cu is removed from the modified surface following the tape test. When a LiF filter, which cuts off wavelengths shorter than 105 nm [17], was placed 3 cm above the FEP and PFA samples, the adhesion failure did not occur until ca. 2 hr of treatment time (Figures 10 – 13)

Figure 14 and 15 shows a series of adhesion results when FEP and PFA samples were treated for 1h and 2 h, respectively, with the Ar flow rate maintained at 20 sccm and the oxygen flow rate was varied between 0-20 sccm.

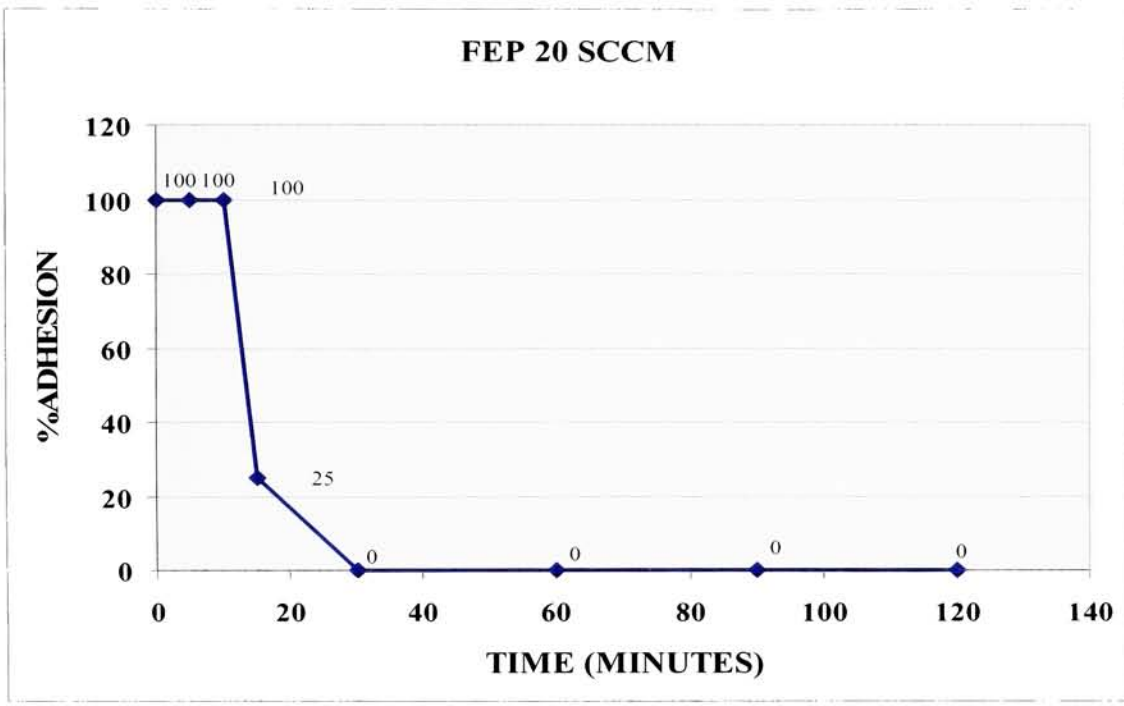

Fig. 6 % Cu adhesion as a function of exposure time for FEP samples treated with 20 sccm flow rates for both Ar and oxygen.

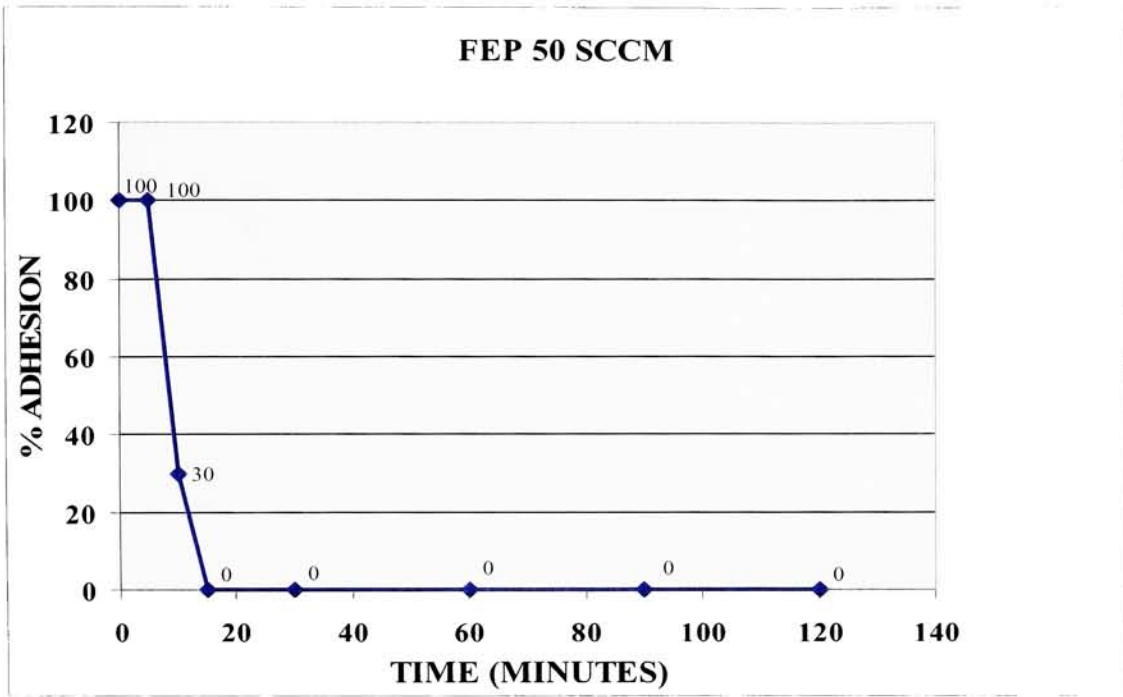

Fig. 7% Cu adhesion as a function of exposure time for FEP samples treated with 50 sccm flow rates for both Ar and oxygen.

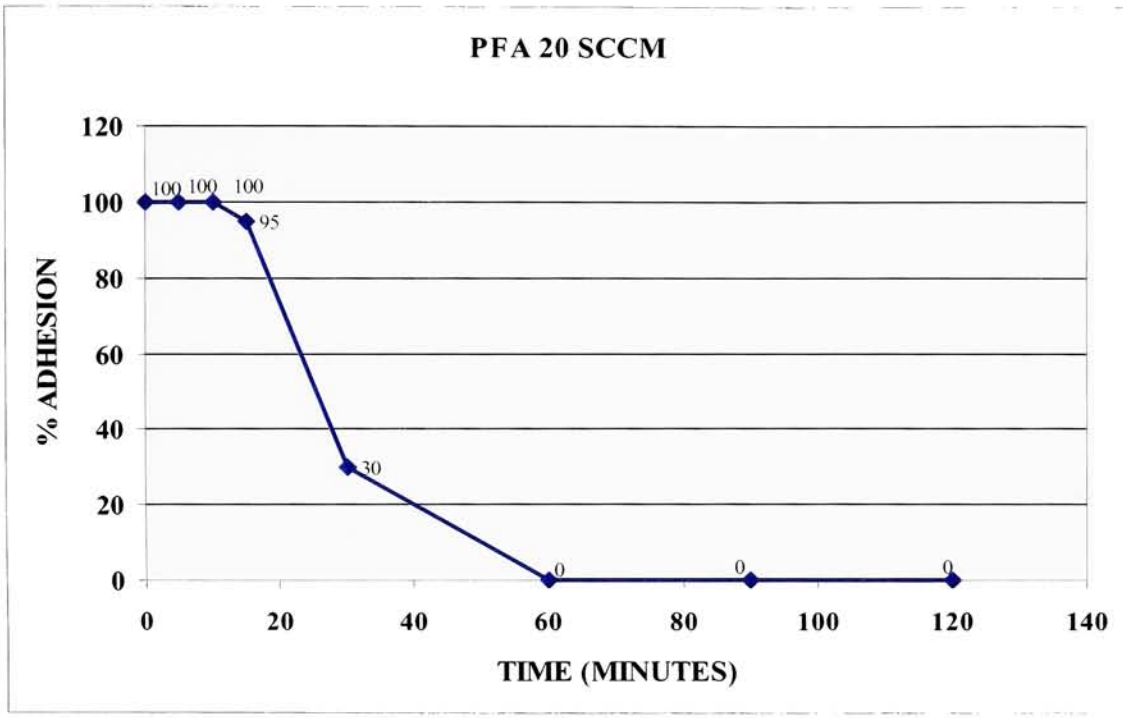

Fig. 8 % Cu adhesion as a function of exposure time for PFA samples treated with 20 sccm flow rates for both Ar and oxygen

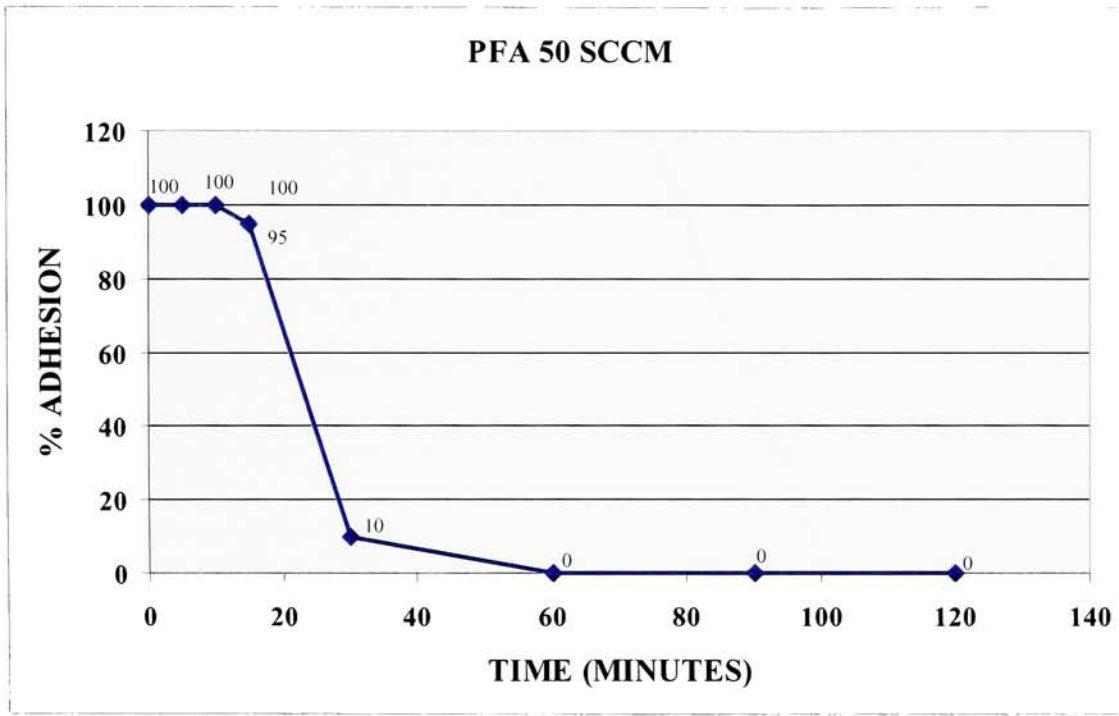

Fig. 9 % Cu adhesion as a function of exposure time for PFA samples treated with 50 sccm flow rates for both Ar and oxygen

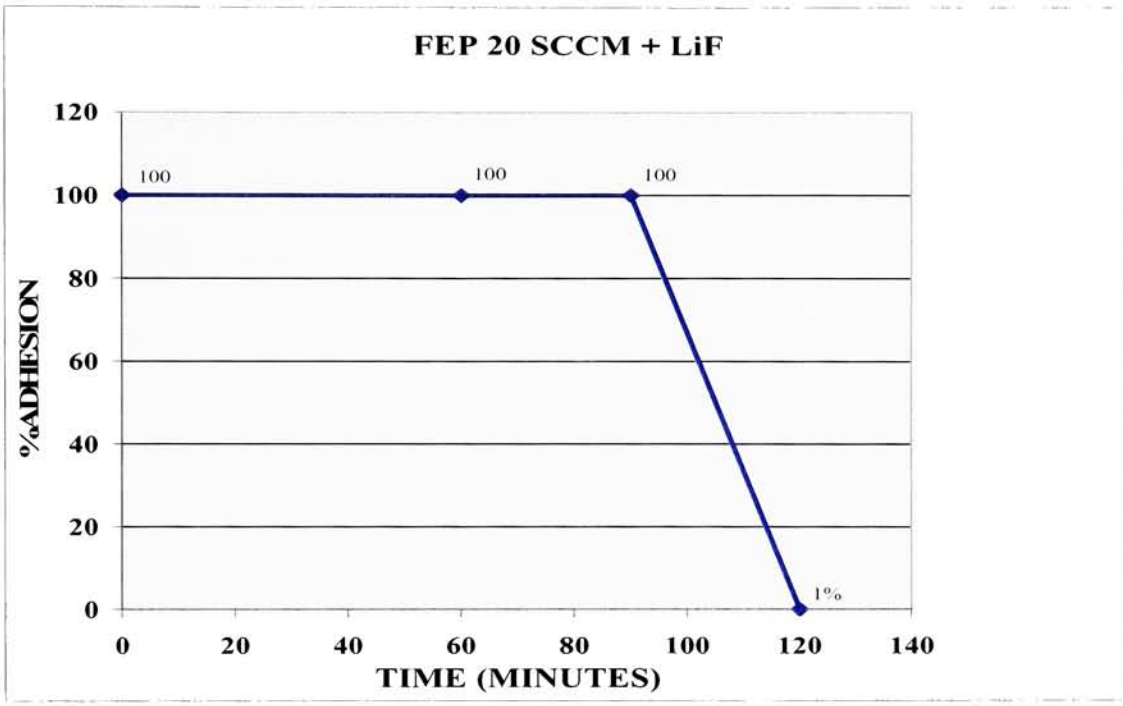

Fig. 10 % Cu adhesion as a function of exposure time for FEP samples treated with 20 sccm flow rates for both Ar and oxygen in the presence of LiF cut off wavelength filter

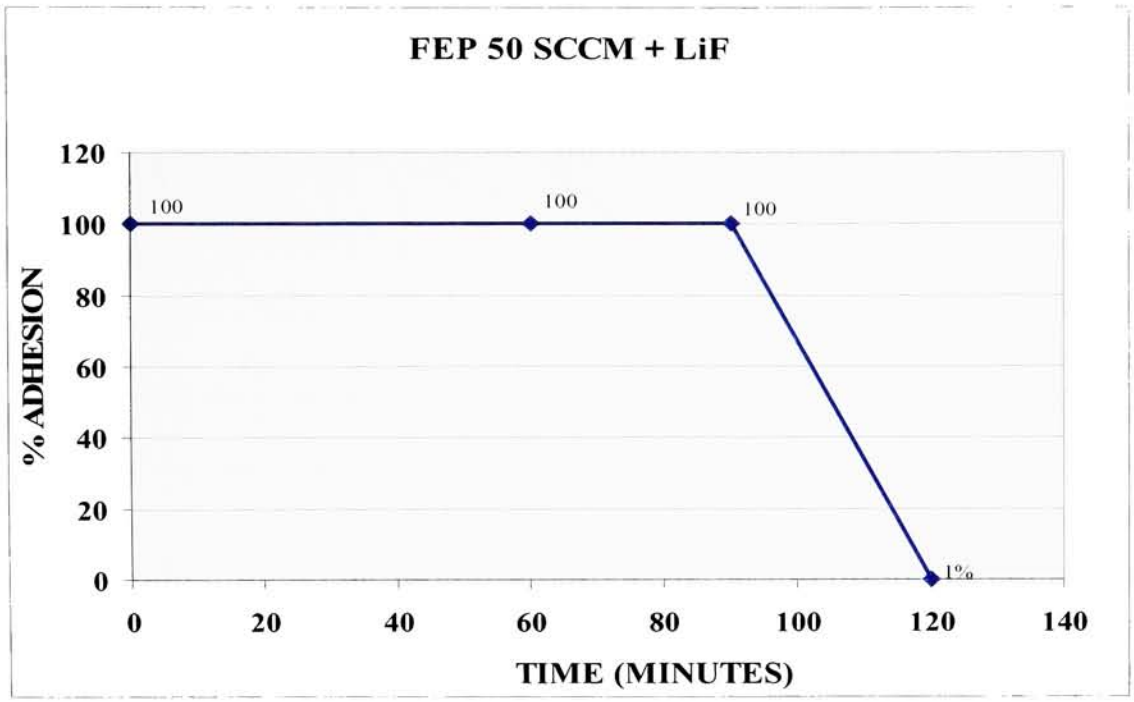

Fig. 11 % Cu adhesion as a function of exposure time for FEP samples treated with 50 sccm flow rates for both Ar and oxygen in the presence of LiF cut off wavelength filter

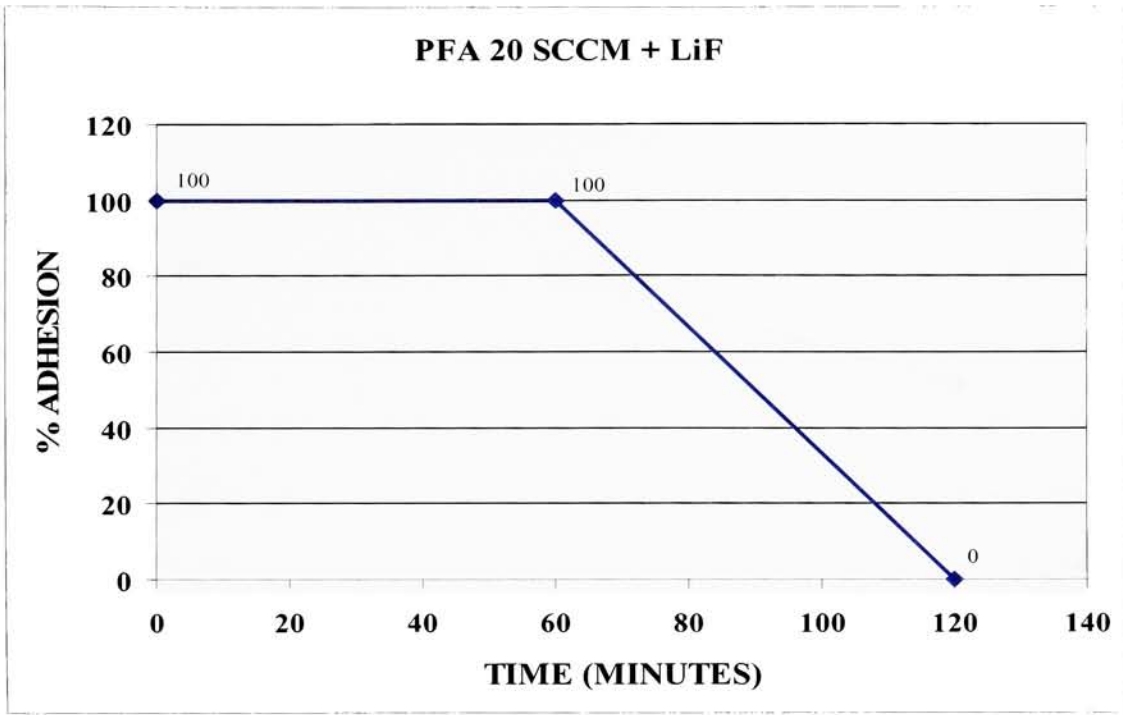

Fig. 12 % Cu adhesion as a function of exposure time for PFA samples treated with 20 sccm flow rates for both Ar and oxygen in the presence of LiF cut off wavelength filter

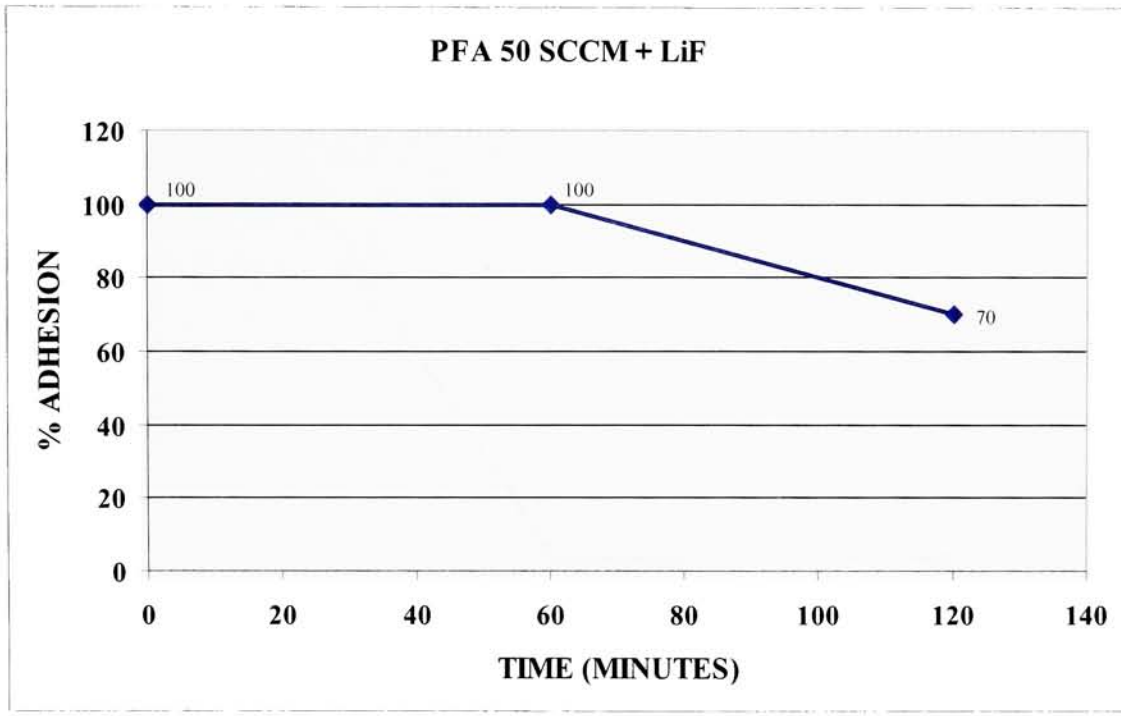

Fig. 13 % Cu adhesion as a function of exposure time for PFA samples treated with 50 sccm flow rates for both Ar and oxygen in the presence of LiF cut off wavelength filter

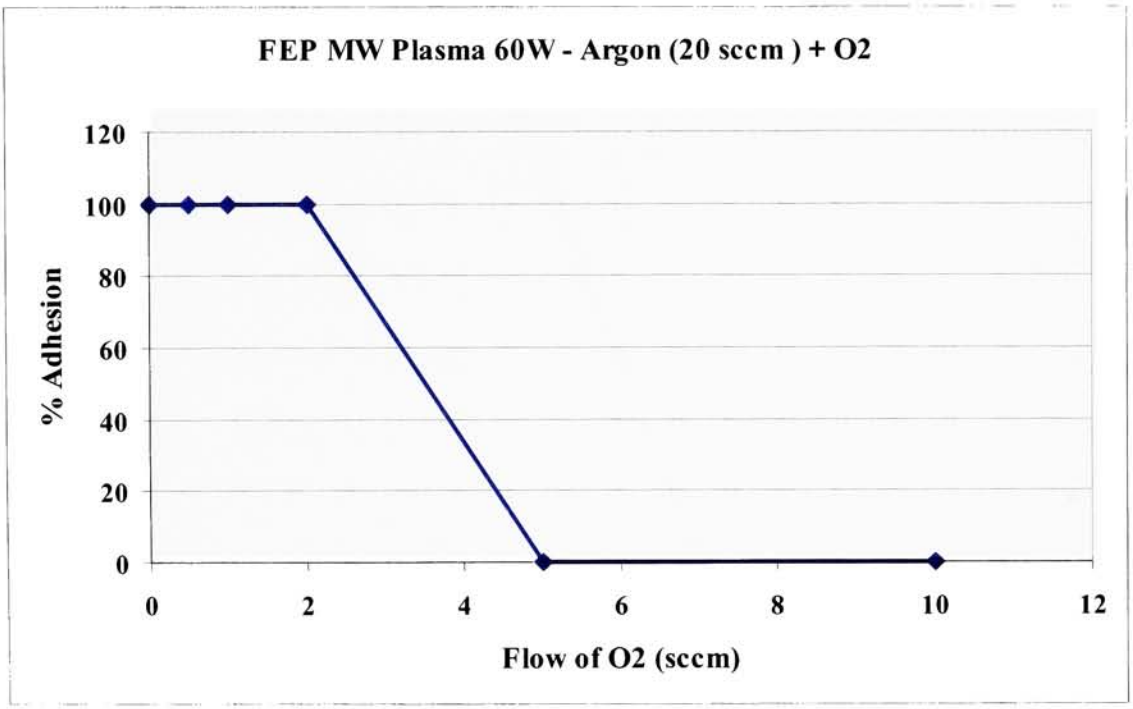

Fig.14 % Cu adhesion as a function of oxygen flow rate for FEP samples treated with VUV radiation from 20 sccm Ar MW plasma for 1 hr.

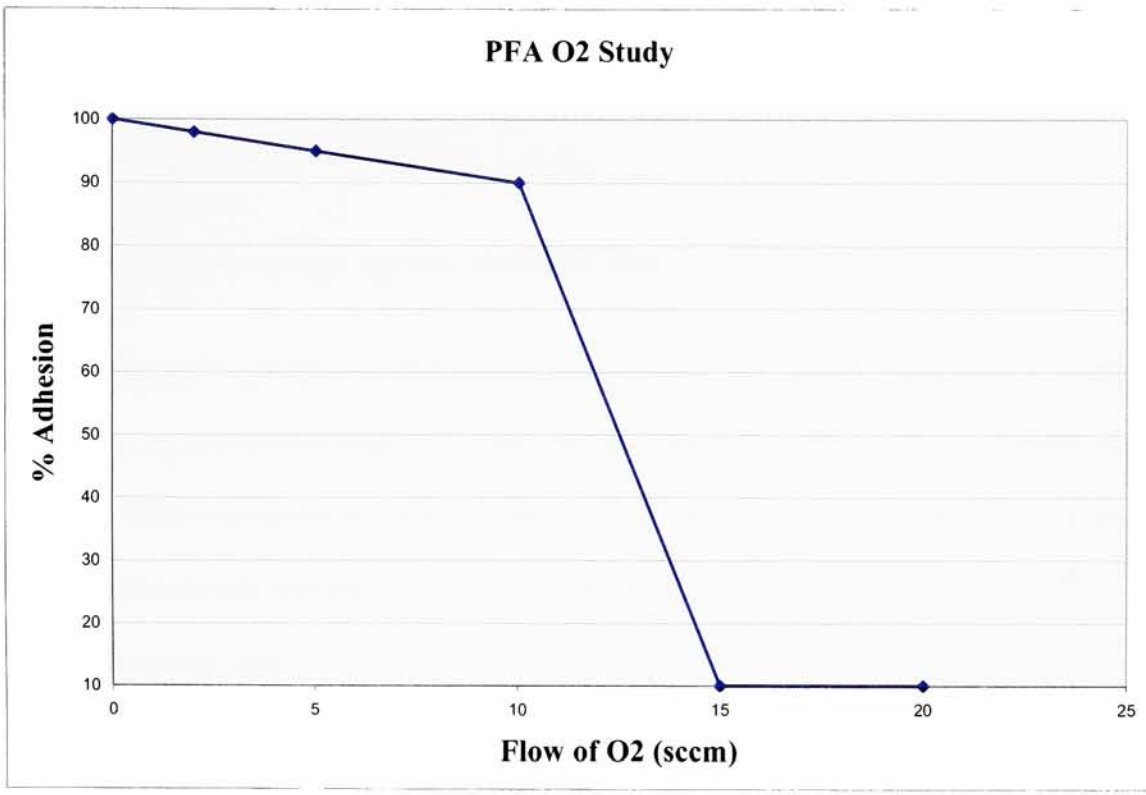

Fig.15 % Cu adhesion as a function of oxygen flow rate for PFA samples treated with VUV radiation from 20 sccm Ar MW plasma for 2 hr.

3.5 XPS results

3.5.1 Qualitative and Quantitative XPS Analyses

The elemental survey scans from 0 to 1000 eV binding energy detected carbon, fluorine and oxygen for all of the FEP and PFA samples.

3.5.2 XPS Analyses for the Surface Modified FEP

Table 2 shows the quantitative XPS results for untreated FEP and FEP treated as a function of treatment time and flow rates of Ar and oxygen. The calculated fluorine to carbon ratios show that treatment results in a small degree of defluorination. The untreated FEP samples contained 0.4 atomic percent oxygen. The treated FEP surfaces contained from 0.9 to 2.1 atomic percent oxygen.

Table 2. Quantitative XPS Results for FEP as a Function of Treatment Time and Flow Rates of Ar and Oxygen

Time Flow Rate	At% C	At% F	At% O	F/C	O/C	O/F
Untreated	32.1	67.5	0.4	2.10	0.012	0.006
2 h 20 sccm	34.3	63.6	2.1	1.85	0.061	0.033
2 h 50 sccm	32.8	65.6	1.6	2.00	0.049	0.024
15 min 20 sccm	33.3	65.3	1.4	1.96	0.042	0.021
10 min 50 sccm	32.6	66.6	0.9	2.04	0.028	0.014

3.5.3 Chemical State Analyses for Treated FEP samples

Figure 16 shows the C 1s spectra, overlapped and normalized, for the untreated and treated samples. The spectra are almost identical. There are slight differences in the intensity of the structure around 294 eV and from 286 to 290 eV due to CF_3 bonding and carbon – oxygen bonding, respectively, which is easier to interpret using the O 1s spectra.

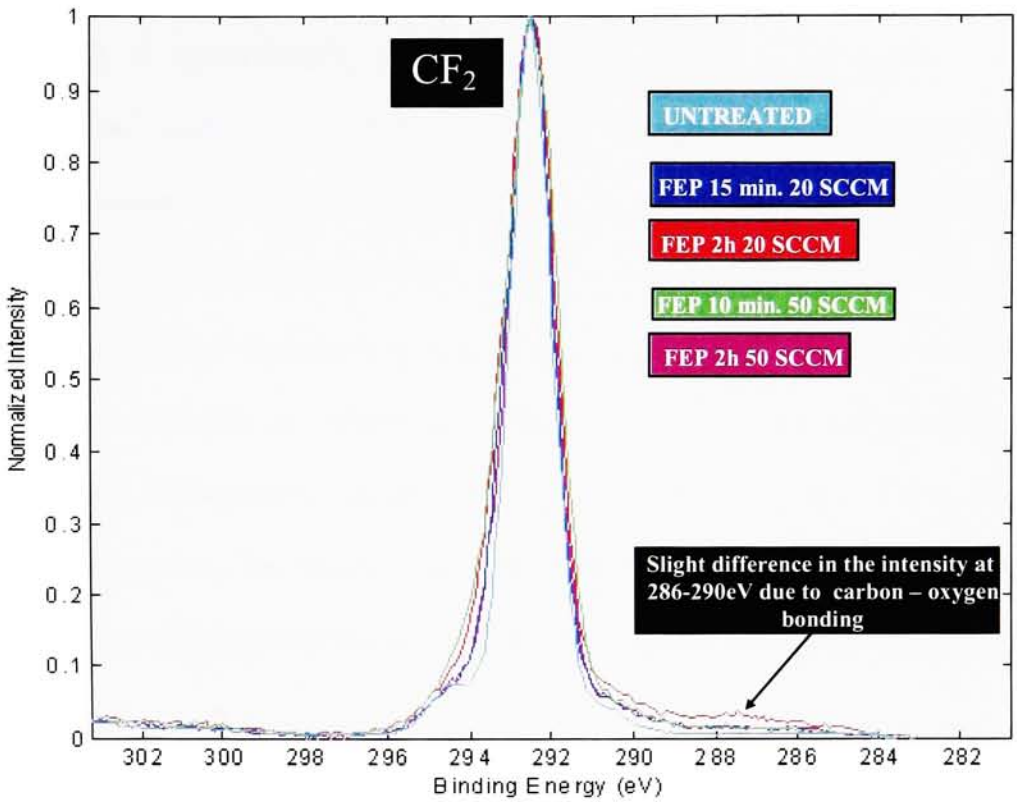

Figure 16. C1s spectra for the FEP untreated (—), treated for 15 min at 20 sccm (—), treated for 2h at 20 sccm (—), treated for 10 min at 20 sccm (—), and treated for 2hr at 50 sccm (—).

Figure 17 illustrates the O 1s spectra, overlapped and normalized, for the untreated and treated FEP samples. The untreated sample yielded two peaks, one peak at 532 eV and another peak at approximately 536 eV due to a CF-O-CF_3 type moiety. Table 3 summarizes the results of curve fitting the spectra. The principal components are peaks that can be assigned to C-O, C=O and CF-O-CF_3 type moieties at the binding energies of 532.4, 533.5, and 536.0 eV, respectively. An excellent fit, chi square less than 1.000, is obtained by including components due to CF-O-CF_2 and CF_2-O-CF_2 moieties at binding energies 534.7 and 535.8 eV, respectively. The error bar for the binding energies is a few tenths of an eV. Chi square is a measure of the goodness of fit of the sum of the peaks used to model the spectrum. The excellent statistical fit indicates that the selection of peaks with their intensities, widths and energy locations replicate the spectroscopic data very well.

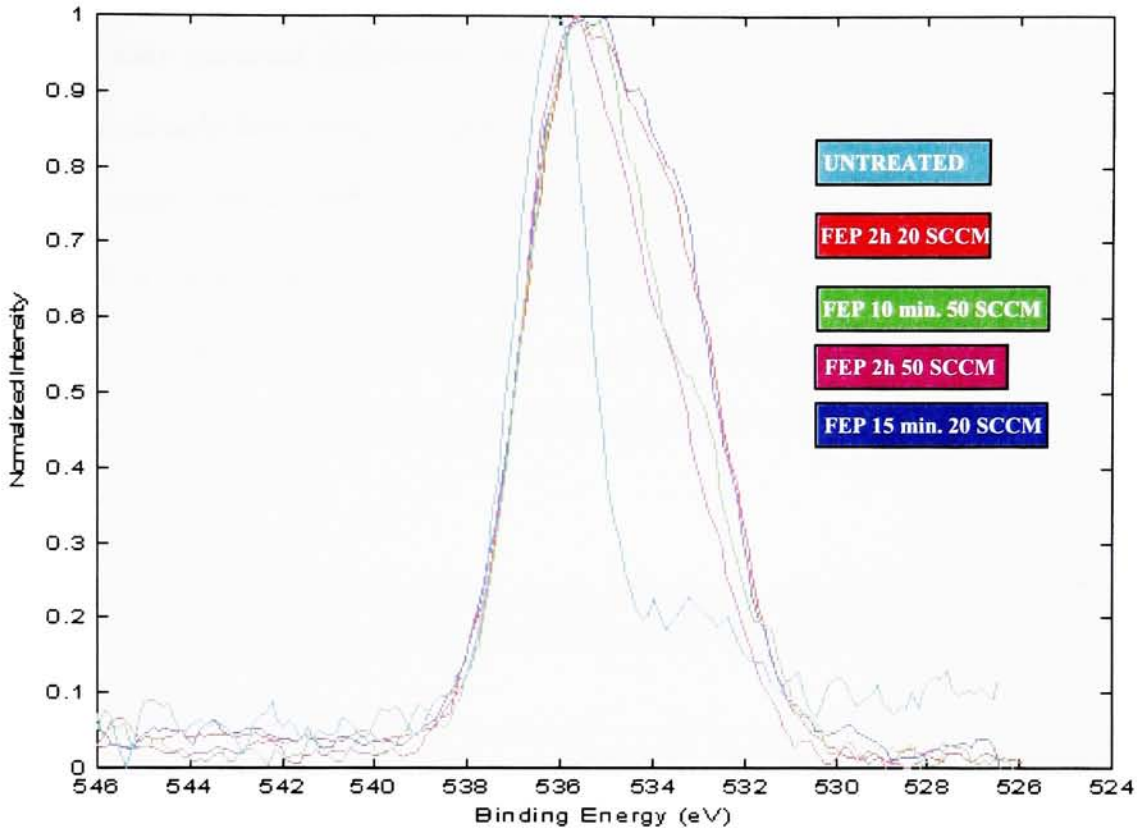

Figure 17. O1s spectra for the FEP untreated (——), treated for 2 hr at 50 sccm (——), treated for 10 min at 50 sccm (——), treated for 15 min at 20 sccm (——), and treated for 2hr at 20 sccm (——).

For the treated samples, the O 1s peaks are similar in shape (Figs. 17). The results of the curve fittings in Table 3 show that the contributions from CF-O-CF_2 and CF_2-O-CF_2 moieties have increased significantly upon treatment. The results in Table 3 cannot be compared directly from sample to sample because the oxygen concentrations for untreated FEP and treated samples differ significantly. A direct comparison can be made by using the results from Table 3 and Table 2 to construct Table 4 which shows the actual oxygen concentrations by species for each sample. In general, treatment of the surface results in an increase in the concentrations of the CF-O-CF_2, CF_2-O-CF_2 and CF-O-CF_3 species.

Table 3. Results of XPS O1s Curve Fitting for FEP Treated Downstream From Ar Microwave Plasma With Flowing Oxygen as a Function of Treatment Time and Flow Rate

Time Flow Rate	**C-O**	**C=O**	**CF-O-CF_2**	**CF_2-O-CF_2**	**CF-O-CF_3**
Untreated	21	21	8	8	41
2 h 20 sccm	9	11	16	25	40
2 h 50 sccm	5	6	14	25	50
15 min 20 sccm	4	5	27	23	41
10 min 50 sccm	7	9	12	27	45

Table 4. Oxygen Distribution for Untreated and Treated FEP Samples as a Function of Treatment Time and Flow Rates of Ar and Oxygen

Time Flow Rate	C-O	C=O	$CF\text{-}O\text{-}CF_2$	$CF_2\text{-}O\text{-}CF_2$	$CF\text{-}O\text{-}CF_3$
Untreated	0.1	0.1	0.03	0.03	0.2
2 h 20 sccm	0.2	0.2	0.3	0.5	0.8
2 h 50 sccm	<0.1	<0.1	0.2	0.4	0.8
15 min 20 sccm	<0.1	<0.1	0.4	0.3	0.6
10 min 50 sccm	<0.1	<0.1	0.1	0.2	0.4

The oxygen distributions for samples treated with VUV radiation and flowing oxygen (Table 4) shows the introduction of oxygen into the structure of FEP. The largest amount is incorporated at 2 hours of exposure as expected. The most oxygen is incorporated at the lower flow rate. This suggests that at a flow rate of 50 sccm the reactive species do not reach the surface of the FEP as effectively as at the lower flow rate. The same is true for the shorter exposure times. The sample treated for 15 minutes at 20 sccm incorporates more oxygen into the structure than the sample treated for 10 minutes, but at the higher gas flow.

3.5.4 XPS evaluation of methods for cleaning PFA

Figure 18 shows the overlapped and normalized C 1s spectra for PFA "as received", cleaned with hexane wash, and cleaned with methanol and acetone treatment. The principal peaks at about 292.5 eV and about 294 eV are due to the CF_2 and CF_3 moieties, respectively. The PFA washed with methanol and acetone shows an enhanced peak due to CF_3 relative to the "as received" PFA. The hexane washed PFA shows very little CF_3 functionality, as well as, a peak at 285 eV due to hydrocarbon C-C bonding because of adsorbed hexane. The "as received" PFA also shows a weak peak due to C-C bonding. The methanol and acetone wash is very effective for the removal of residual hydrocarbon. There are also peaks at 286 and 289 eV which are characteristic of C-O bonding. The peak at 286 eV is due to carbon singly bonded to one oxygen atom in the structure while the peak at 289 eV is due to carbon bonded to two or more oxygen atoms.

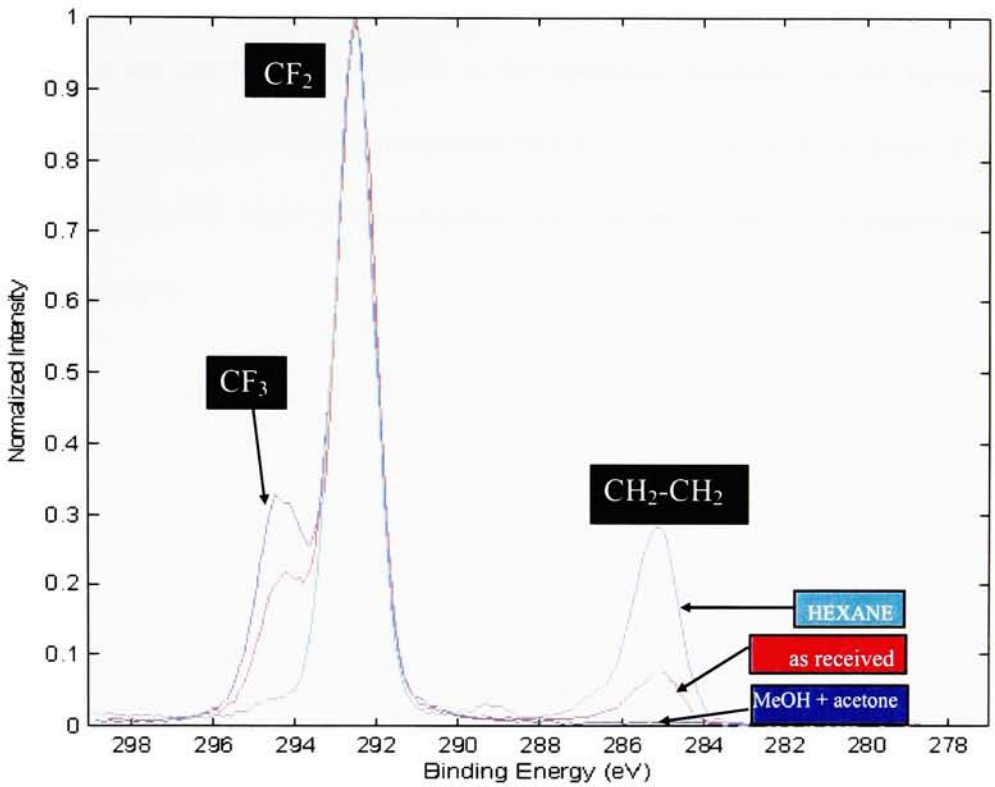

Fig. 18 C1s spectra for the as "received" (—), washed with methanol and acetone (—) and washed with hexane (—) PFA films

The O 1s spectra are shown in Figure 19. The peak at about 536 eV is due to CF_2-O-CF_2 moiety that is present in PFA and is the dominant peak in the spectra for the "as received" and methanol and acetone washed PFA films. The peaks due to polycarbonate/maleic anhydride-like oxygen atoms dominate in the spectrum acquired for the hexane washed PFA film where carbonyl appears at around 532.4 eV and O-C=O* at about 534 eV. All samples modified with VUV photo-oxidation were cleaned with the methanol and acetone washing procedure.

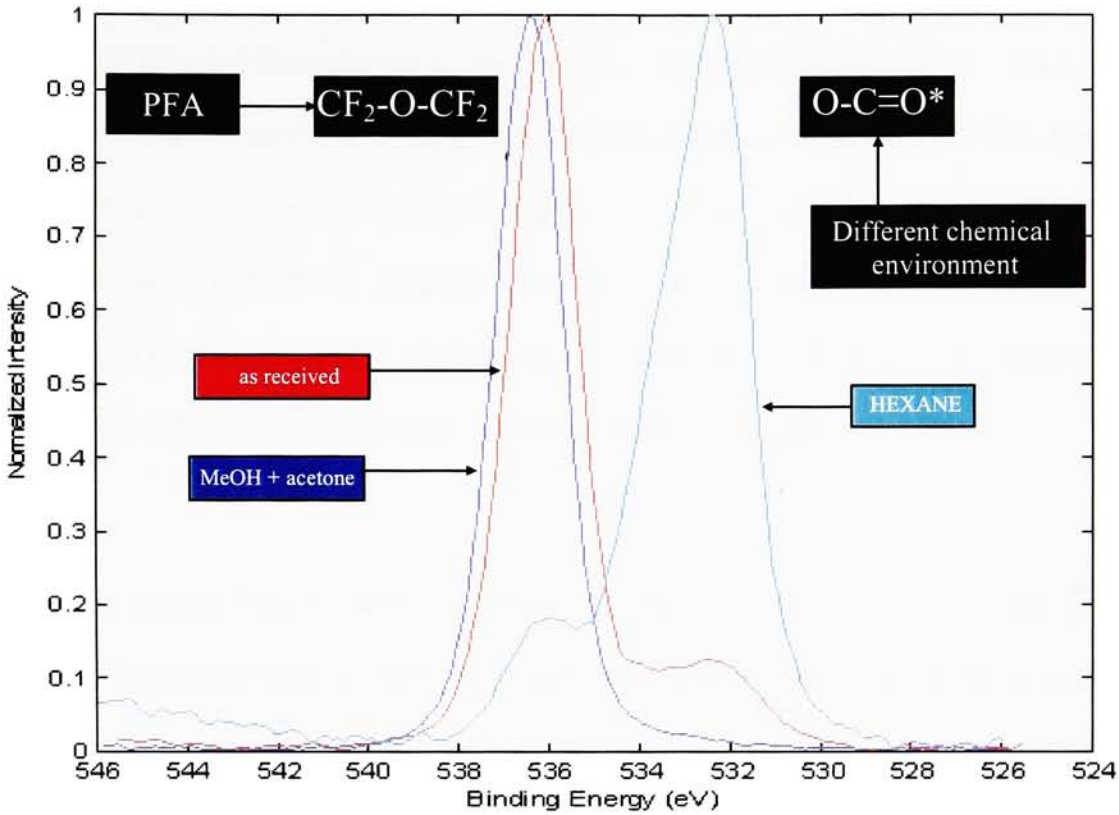

Fig. 19 O1s spectra for the as "received" (—), washed with methanol and acetone (—) and washed with hexane (—) PFA films

3.5.5 XPS analyses of surface modified PFA

Table 5 shows the quantitative XPS results for untreated PFA and PFA treated as a function of time and flow rates of Ar and oxygen. The calculated fluorine to carbon ratios show that treatment results in a small degree of defluorination. The untreated PFA samples contained 0.2 - 0.6 atomic percent of oxygen. The lower values were achieved by using additional steps beyond the washing procedure, such as, vacuum oven drying and/or pumping on the sample prior to starting the MW discharge or abrasion of the sample. The treated PFA surfaces contained up to 2.7 atomic percent of oxygen.

The C 1s spectra, Fig. 20, were overlapped and normalized for the control and treated samples. The spectra were found to be almost identical except for slight differences in the intensity of the structure around 294 eV and from 286 to 290 eV due to CF_3 bonding and carbon – oxygen bonding, respectively. The interpretation of the bonding was easier to resolve using the O 1s spectra, as shown in Fig. 21 for 2 h treatment at flow rates of 20 and 50 sccm. The principal components of the spectra include contributions from methanol, acetone, PFA and surface-modified PFA. An excellent curve fit is obtained, with a chi squared less than 1.00, by including components due to CF-O-CF_2 and CF_2-O-CF_2 moieties at binding energies 534.7 and 535.8 eV, respectively, along with C-O, C=O and CF-O-C_nF_{2n+1} type moiety at the binding energies of 532.4, 533.5, and 536.0 eV, respectively. The error bar for the binding energies is a few tenths of an eV. Table 6 shows that photo-oxidation significantly increases the contributions from CF-O-CF_2 and CF_2-O-CF_2. Since the oxygen concentrations differ substantially with the samples, a direct comparison was achieved by using the results from Table 6 and Table 5 to create Table 7 which shows the

actual oxygen concentrations by species for each sample. The results in Table 7 clearly show that all carbon-oxygen species, with the exception of C-O, increase with treatment. The C-O moiety is assumed to be due to residual methanol.

Table 5. Quantitative XPS Results for PFA as a Function of Treatment Time and Flow Rate for Ar and Oxygen

Time/ Flow Rates	C At%	F At%	O At%	F/C	O/C	O/F
Washed	33.3	66.2	0.6	1.99	0.018	0.009
Washed	33.6	65.9	0.6	1.96	0.018	0.009
45 min Vac	33.3	66.4	0.3	1.99	0.009	0.005
Washed	33.3	66.3	0.5	1.99	0.015	0.008
30 minVac	32.8	66.7	0.4	2.03	0.012	0.006
15 min/20 sccm	33.4	66.1	1.5	1.98	0.045	0.023
15 min/50 sccm	33.5	64.4	1.9	1.92	0.057	0.029
45 min/20 sccm	32.4	65	2.6	2.01	0.08	0.04
45 min/20 sccm	34.2	64.2	1.6	1.88	0.047	0.025
45 min/50 sccm	33.6	64.2	2.3	1.91	0.068	0.036
45 min/50 sccm	34	63.9	2.0	1.88	0.059	0.031
1 h/20 sccm	32.9	64.4	2.7	1.96	0.082	0.042
1 h/50 sccm	36.2	61.7	2.2	1.7	0.061	0.036
1 h/20 sccm	33.4	65.1	1.4	1.95	0.042	0.022
2 h/20 sccm	33.4	64.5	2.1	1.93	0.063	0.033
2 h/20 sccm	33.1	65.7	1.2	1.98	0.036	0.018
2 h/20 sccm	32.9	65.2	1.9	1.98	0.058	0.029
2 h/20 sccm	32.7	65.5	1.8	2	0.055	0.027
2 h/50 sccm	34.8	63.6	1.6	1.83	0.049	0.025
2 h/50 sccm	32.9	64.9	2.2	1.97	0.067	0.034

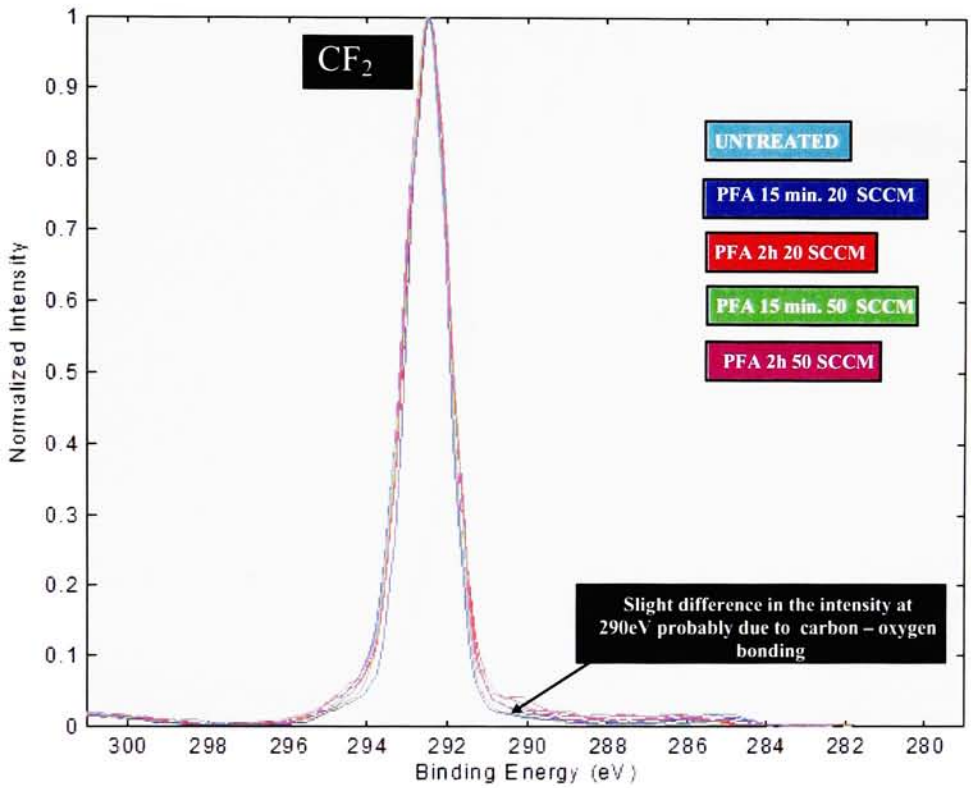

Figure 20. C1s spectra for the PFA untreated (—), treated for 15 min at 20 sccm (—), treated for 2h at 20 sccm (—), treated for 15 min at 50 sccm (—), and treated for 2hr at 50 sccm (—)

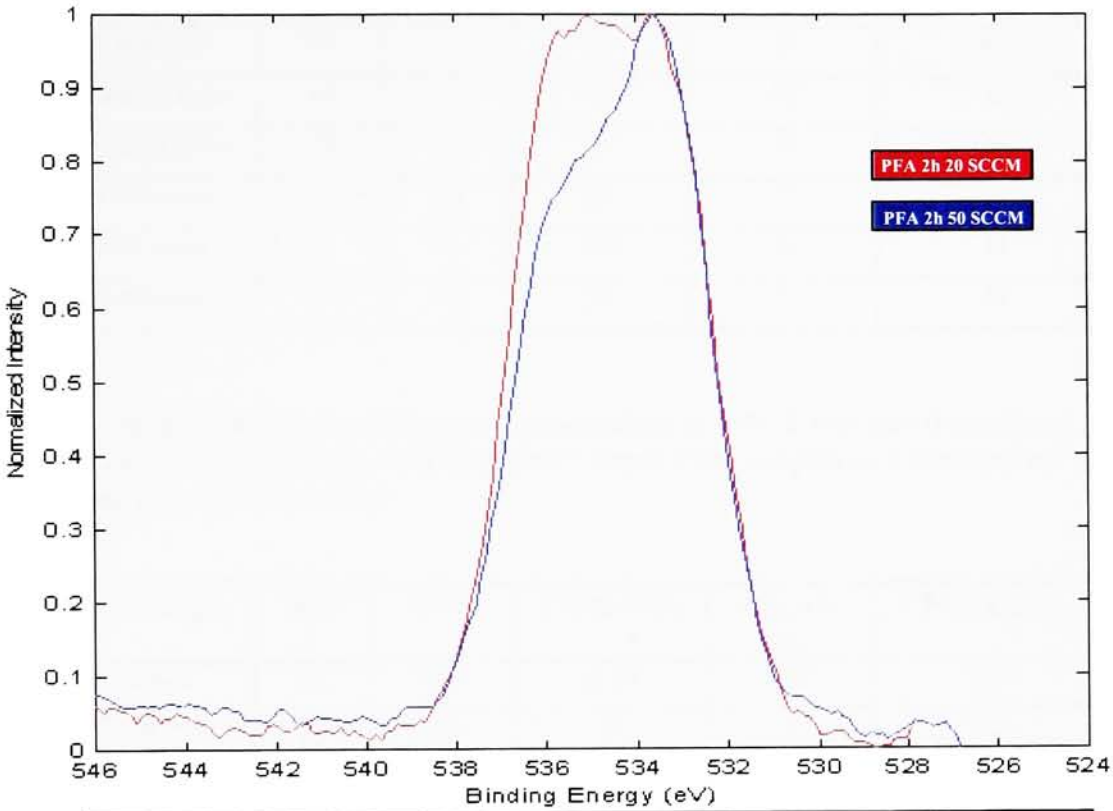

Fig. 21 O1s XPS spectra for PFA:treated for 2hr at 20 sccm (—) and 50 sccm (—)

Table 6. XPS Results of O1s Curve Fitting for PFA Treated Downstream From Ar Microwave Plasma With Flowing Oxygen as a Function of Treatment Time and Flow Rate

PFA Sample	C-O	C=O	CF-O-CF_2	CF_2-O-CF_2	CF-O-C_nF_{2n+1}
Washed	23	22	7	12	36
30 min vac	30	26	0	0	44
15 min/20 sccm	16	14	19	19	32
15 min/50 sccm	14	15	19	19	33
1h /50 sccm	4	16	25	23	32
2h/20 sccm	5	16	24	20	34
2h/50sccm	5	18	28	19	30

Table 7. Oxygen Distribution (Oxygen Concentration in At% X Fraction from Curve Fitting Results in Table 6) for Untreated and Treated PFA Samples as a Function of Treatment Time and Flow Rate

PFA Sample	C-O	C=O	CF-O-CF_2	CF_2-O-CF_2	CF-O-C_nF_{2n+1}
Washed	0.1	0.1	0.04	0.07	0.3
30 min vac	0.1	0.1	0	0	0.2
15 min/20 sccm	0.2	0.2	0.3	0.3	0.5
15 min/50 sccm	0.2	0.3	0.4	0.4	0.6
1h/50 sccm	<0.1	0.3	0.6	0.5	0.7
2h/20sccm	0.1	0.3	0.5	0.4	0.6
2h/50sccm	0.1	0.4	0.6	0.4	0.7

3.5.6 XPS results after adhesion test

When adhesion failure occurred, XPS analysis was conducted on both failure surfaces, i.e., the Cu-side and polymer-side. Copper was not detected on either side of the tape. The detected oxygen concentrations, as shown in Table 8 for FEP and Table 9 for PFA, were similar to the untreated surface indicating that the failure was cohesive and occurred within the polymer and not at the Cu-polymer interface.

Table 8. XPS Results on FEP-side and Cu-side after Peel Test on FEP Treated Downstream from 60W Ar Microwave Plasma with Flowing Oxygen as a Function of Treatment Time and Flow Rates of Ar and Oxygen

Side Analyzed Time Flow Rate	**At% C**	**At% F**	**At% O**	**F/C**	**O/C**	**O/F**
Untreated	32.1	67.5	0.4	2.10	0.012	0.006
FEP-side 2 hr 20 sccm	32.8	66.8	0.5	2.04	0.015	0.007
Cu-side 2 hr 20sccm	31.8	67.5	0.7	2.12	0.022	0.010
FEP-side 2 hr 50 sccm	32.7	67.0	0.4	2.05	0.012	0.006
Cu-side 2 hr 50 sccm	32.5	66.6	0.9	2.05	0.028	0.014
FEP-side 15 min 20 sccm	32.2	67.5	0.3	2.10	0.009	0.004
Cu-side 15 min 20 sccm	32.8	66.7	0.5	2.03	0.016	0.007
FEP-side 10 min 50 sccm	32.0	67.7	0.3	2.12	0.009	0.004
Cu-side 10 min 50 sccm	31.9	67.7	0.4	2.12	0.013	0.006

Table 9. Quantitative XPS Results of Failure Surfaces after Tape Adhesion Test for treated PFA samples

Tape Side Time Flow Rate	C At%	F At%	O At%	F/C	O/C	O/F
Untrated	33.3	66.2	0.6	1.99	0.018	0.009
PFA-side 45 min 20 sccm	32.9	66.7	0.3	2.03	0.009	0.004
Cu-side 45 min 20sccm	33.9	65.4	0.6	1.93	0.018	0.009
PFA-side 45 min 20 sccm	33.0	66.7	0.4	2.02	0.012	0.006
Cu-side 45 min 50 sccm	33.6	67.1	0.4	2.06	0.012	0.006
PFA-side 2 hr 20 sccm	32.0	67.6	0.4	2.11	0.013	0.006
Cu-side 2 hr 20sccm	33.4	65.9	0.7	1.97	0.021	0.011
PFA-side 2 hr 50 sccm	33.1	66.5	0.4	2.01	0.012	0.006
Cu-side 2 hr 50 sccm	33.1	66.3	0.5	2.00	0.015	0.008
PFA-side 2 hr 20 sccm	32.0	67.6	0.4	2.11	0.013	0.006
Cu-side 2 hr 20sccm	33.4	65.7	0.9	1.97	0.027	0.014
PFA-side 2 hr 50 sccm	32.7	67.0	0.3	2.05	0.009	0.004
Cu-side 2 hr 50 sccm	33.4	65.8	0.8	1.97	0.024	0.012

4. DISCUSSION

The photo-absorption spectrum of FEP has an intense band at 7.7 eV (160 nm), with a weak absorption tail at the low energy side and a rising continuous absorption with fine structures at the high energy side [33]. With the very small perfluoropropyl vinyl ether content in PFA, the shape of the photo-absorption spectrum of PFA is expected to be similar to PTFE [34] and FEP [33]. The energies associated with the VUV photons emitted from the excited Ar atoms at 104.8 and 106.7 nm may initiate significant chemical effects to produce free radicals (R•) and ions (R^+). Since the photon energies are greater than the C-C (~3 eV), C-F (~5 eV) [35, 36], C-O bond strength (~4 eV) [37], and the estimated first ionization potential (~11 eV) [38], reaction steps (3)-(5) are energetically possible in the present study.

$$\text{Fluoropolymer} + h\nu = R_1\bullet + R_2\bullet \qquad \lambda \leq 410 \text{ nm} \qquad (3)$$

$$\text{Fluoropolymer} + h\nu = R_3\bullet + F\bullet \qquad \lambda \leq 250 \text{ nm} \qquad (4)$$

$$\text{Fluoropolymer} + h\nu = \text{Fluoropolymer}^+ + e^- \qquad \lambda \leq 120 \text{ nm} \qquad (5)$$

For PFA the following reaction step is also possible:

$$\text{PFA} + h\nu = R_3\bullet + R_4O\bullet \qquad \lambda \leq 310 \text{ nm} \qquad (6)$$

The observation of negligible photo-etching (≤1 nm/min) for FEP and PTFE [17] is probably a result of the low intensity of VUV radiation present downstream from the MW

Ar source. The intensity of radiation is dependent on the amount of photo-absorption of the photons by the rare gas (resonance self-absorption) in the distance between the source and the sample. Several investigators have previously reported erosion of FEP with more intense VUV radiation sources including: continua from windowless Ar (105-155 nm) and He (58-110 nm) excimers [39], 124 and 147 nm [33, 40], $\geq$ 115 nm [41] and 157.6 nm radiation from a F_2 laser [42]. Exposure of FEP to high UV radiation fluences at $\geq$ 190 nm results in only slight photo-degradation because of the small photo-absorption coefficients at these wavelengths [43].

The advancing DI water contact angles on the modified FEP and PFA surface presented in Fig. 2 and 3 are similar to those obtained for photo-oxidation of PTFE downstream from He and Ar microwave plasmas [17]. Treatment of PFA for 60 min with the more energetic VUV photons from a 1.0 kW He MW plasma followed by exposure to air resulted in an advancing contact angle of 63° [18]. Contact angle measurements are very surface sensitive, in contrast, VUV radiation emitted by a F_2 excimer laser pulse at 157.6 nm has a substantial penetration depth (distance at which the incident intensity has decreased to 1/e of the initial value) within FEP of ca. 520 nm [33], although, a penetration depth of only ~0.1 nm at a wavelength of 125 nm has been reported for the more opaque and polycrystalline PTFE [44].

Contributions from the photochemical effects due to photo-absorption by oxygen need to be considered in the surface modification of FEP and PFA, when oxygen is flowing over the surface of the polymer since oxygen absorbs strongly in the VUV region of the

electromagnetic spectrum [45]. Photochemical steps (7)-(9), which produce ground, ^3P, and electronically excited, ^1D and ^1S, oxygen atoms, are energetically possible using the Ar MW source [46].

$$O_2 + h\nu = O(^3P) + O(^3P) \quad \lambda \leq 242.4 \text{ nm} \qquad (7)$$

$$O_2 + h\nu = O(^3P) + O(^1D) \quad \lambda \leq 175 \text{ nm} \qquad (8)$$

$$O_2 + h\nu = O(^3P) + O(^1S) \quad \lambda \leq 133.2 \text{ nm} \qquad (9)$$

The neutral Ar resonance lines at 104.8 and 106.7 nm occur within a region of the oxygen absorption spectrum where the Rydberg series converges towards the first ionization potential [47]. Measured photo-absorption coefficients of oxygen at 104.91 and 106.60 nm have values of 61 and 101 cm^{-1} that correspond to photo-absorption cross-sections of 2.27 $x10^{-18}$ and 3.75 $x10^{-18}$ cm^2, respectively [47]. Coupling these cross-sections with parameters pertinent to the experiments in this study (the oxygen number density and pathlength through the oxygen, 3 cm), more than 93% of the VUV radiation from the Ar MW discharge is transmitted through the oxygen to modify the FEP surface.

Figure 4 (b) and 5 (b) shows enhanced roughening of the surface when FEP and PFA is treated downstream from the Ar plasma compared to the untreated sample (Fig. 4 (a) and 5 (a)). Reactions of the VUV photons, as well as of molecular oxygen and oxygen species formed in steps (7)-(9) with the surface free radical sites, contribute to the surface

roughness. Ground state oxygen atoms, $O(^3P)$, created either by reaction steps (7)-(9) or deactivation of electronically excited oxygen atoms, may combine with oxygen molecules to produce ozone that oxygenates the surface reactive sites. $O(^1S)$, which is formed in reaction step (9) and is 4.189 eV above the ground state [46], may also directly abstract a F atom from FEP and PFA by reaction step (10) since the analogous reaction involving ground state oxygen atoms is endothermic by only about 3.2 eV.

$$O(^1S) + CF_4 = OF + CF_3 \qquad (10)$$

Because changes in contact angle are very surface sensitive, the observed changes may arise from surface roughening (Figs. 4 (b) and 5 (b)) in addition to chemical modification. Scanning electron micrographs of FEP surfaces exposed to VUV and atomic O on the high altitude long duration exposure facility also show considerable roughening [48-50].

Enhancement of roughening may also be due to differences in reactivity between amorphous and crystalline regions of the polymer.

The XPS results (Table 2) for untreated FEP show 0.4 atomic percent oxygen as compared to a previously reported value of 0.6 [39]. The oxygen may be due to introduction during processing [51] and/or residual amounts of the solvents used for washing the samples. Pumping on the washed untreated sample for 30 min reduced the atomic oxygen concentration to 0.3%. Exposing FEP to VUV photo-oxidation downstream from an Ar plasma (Table 2) resulted in subtle defluorination of the surface probably via $C\text{-}CF_3$ and C-

F bond breakages as illustrated in reactions (3) and (4), respectively. Oxygen was detected on the surface at a concentration up to ca. 2 At% similar to the previous results for VUV photo-oxidation of PTFE [17].

The curve fitting of the O1s XPS spectra (Fig. 17 and Table 4) shows that oxygen is inserted into the backbone of the FEP and replaces fluorine and CF_3 that was lost during defluorination. The results of the curve fitting suggest disruption of the backbone of the FEP. There is evidence for insertion of oxygen into the backbone, defluorination and formation of carbon – oxygen bonds in CF-O-CF_2, CF_2-O-CF_2 and CF-O-CF_3 moieties.

The XPS results (Table 5) for untreated PFA show ca. 0.5 atomic percentage of oxygen. With additional steps beyond the washing procedure, such as, vacuum oven drying, pumping on the sample in the vacuum chamber prior to starting the MW discharge or abrasion of the sample, the O At% could be reduced to 0.2% corresponding to an O/C ratio of 0.006. Previously reported values for O/C for untreated PFA include: 0.003 [18], 0.012 [51], <0.05 [6], 0.01 [13], ~0.01 [52], 0.04 [15] and 0.004 [9, 14]. The variability of the O/C values may be due to surface contamination (e.g., Figs. 18 and 19) or the presence of residual solvent from cleaning.

Exposing PFA to VUV photo-oxidation downstream from an Ar plasma (Table 5) resulted in subtle defluorination of the surface probably via C-C, C-O and C-F bond breakage as illustrated in reactions (3) - (6), respectively. Oxygen was detected on the surface at a concentration up to 2.7 At% and O/C= 0.082 similar to previous results for VUV photo-

oxidation of PTFE [17] downstream from an Ar MW plasma with an absorbed power of 60W. Treatment of PFA for 60 min with more energetic VUV photons from a 1.0 kW He MW plasma followed by exposure to air resulted in more extensive defluorination (F/C= 0.50) and incorporation of oxygen (O At%=16.2 and O/C= 0.32) [18].

The curve fitting of the O1s XPS spectra (Fig. 21, Table 6) shows that oxygen is inserted into the backbone of the PFA since there is evidence for the CF-O-CF_2 and CF_2-O-CF_2 moieties in addition to CF-O-C_nF_{2n+1} which is present in the PFA structure.

Momose et al. [53] investigated surface modification of PFA and PTFE with Ar plasma treatment in a radio frequency generator, where VUV radiation is one of the components of the plasma, and subsequent air exposure using XPS and electron spin resonance (ESR). Peroxy radicals (ROO•) were observed with the development of a heavily cross-linked or branched structure incorporating oxygen at the surface. The peroxy radicals were attributed to two types of oxygen: one bonded to carbon in the cross-linked structures mostly at the surface and the other bonded to carbon arising from scission of the main chain mainly in the bulk of the polymer.

Rasoul et al. [51] investigated UV photodegradation of FEP and PFA using a high power xenon lamp at wavelengths greater than 200 nm and also observed by ESR chain scission free radicals, -CF_2•, which were transformed to peroxy radicals, -CF_2OO•, upon exposure to air. XPS analysis showed about a 2 At% of oxygen in the surface due to the formation of C=O groups along with the possible formation of cross-links between polymer chains [51] probably resulting from reactions (10) and (11), respectively [39].

$$R_1OO\bullet + R_2\bullet = R_1O + R_2O \qquad (10)$$

$$R_1\bullet + R_2\bullet = R_1\text{-}R_2 \qquad (11)$$

Analogous to the results in this thesis , exposure of FEP and PFA to VUV radiation in the presence of atomic oxygen resulted in defluorination and an increase in the percentage of carbon attached to oxygen [51]. For FEP a decrease in the percentage of CF_2 and a subsequent increase in the percentages of CF and CF_3 suggests oxidation had occurred preferentially at the fluorinated ethylene units [51] Reaction of atomic oxygen with free radicals produced from the photo-dissociation steps (3-5) would produce fluorinated alkoxyl radicals via reaction step (12) that may react to incorporate oxygen into the polymer chain by reaction (13).

$$R_1\bullet + O = R_1O\bullet \qquad (12)$$

$$R_1O\bullet + R_2\bullet = R_1OR_2 \qquad (13)$$

Fluorinated alkoxyl radicals formed in step (12) and as intermediates in step (10) have been reported to undergo chain scission through a weakened C-C bond to form carbonyl fluoride groups (14) [54, 55].

$$R_1O\bullet = \text{-}CF_2\text{-}CF_2\bullet + \text{-}CF_2C(O)F \qquad (14)$$

Photo-oxidation of FEP using 147 nm VUV radiation from resonance Xe lamps in the presence of 2.5 Torr air has been reported to predominantly produce the carbonyl fluoride groups while treatment with 0.5 Torr air results in the formation of double bonds as observed using FTIR-ATR [54] presumably via decomposition of energetically excited radicals (15) [39].

$$R_1{}^{*\bullet} = \text{-C=C-} + R\bullet \qquad (15)$$

A number of mechanisms at the interface are probably participating in the adhesion of sputter deposited Cu to polymer. The larger electronegativity for the CF_3 group in FEP and C_3F_7O in PFA than CF_2 group in PTFE accounts for the larger measured peel strength for sputter-coated Cu on FEP and PFA compared to PTFE [56]. For untreated materials, following the tape test, nearly all of the sputter-coated copper remained on the surface of FEP and PFA and was removed from PTFE. The observed increase in surface area due to roughening of the surface would contribute to the adhesion. The detected defluorination and oxidation of the VUV modified surface should add to the adhesion strength with copper as has been found for PTFE exposed to He and Ar plasmas and then exposed to air [16, 56], VUV photo-oxidation [17], and mild surface oxidation using a remote oxygen plasma [12]. Defluorination, which is represented by a decrease in the F/C ratio was observed to correlate well with the % Cu adhesion and the increased wettability for modified PTFE surfaces [17]. In addition, cross-linking on the surface caused by treatment, such as VUV photons, may result in increased bondability to FEP and PFA [20, 58-60].

With long treatment times (Figs. 6-9), cohesive failure of the copper sputter-coated onto the modified FEP and PFA surface occurred within the modified polymer film and not at the interface. This may be due to extensive crosslinking near the FEP and PFA surface and chain scission within the sample to weaken the mechanical properties. Polychromatic light from deuterium lamps is also known to penetrate deep into FEP, especially in the VUV regions from 130-140 and 165-175 nm, leading to deterioration in the mechanical properties of FEP [40]. Severe embrittlement (higher surface hardness and induced cracks during bending) has been observed on FEP exposed to solar VUV radiation while serving as the outer layer for thermal blankets on spacecraft in low earth orbit [48]. AFM scratching depth studies revealed that the depth of wear significantly increased after VUV photo-oxidation of FEP in air possibly due to chain scission and depth of penetration of active oxygen species (O, O_3, and O_2*) into the polymer surface [54, 61]. The locus of adhesion failure between Cu and FEP modified with a remote oxygen plasma occurred not at the interface but in the plasma-modified FEP layer near the interface [12]. The presence of weaker CF_3-C bonds in FEP compared to stronger C_3F_7O-C and F-C bonds in PFA resulted in cohesive failure occurring more quickly in FEP than in PFA.

VUV photo-oxidation of PTFE [17] resulted in an increase in the adhesion of Cu to the modified surface and did not appear to exhibit cohesive failure like in FEP and PFA. The pendant trifluoromethyl and perfluoropropoxy groups in FEP an PFA, respectively, result in a greater amorphous character to FEP and PFA contributing to higher rates of cross-linking at the surface and chain scission within the polymer producing cohesive failure compared to the more polycrystalline PTFE which is be expected to be less reactive and

scatter more radiation. A similar explanation was previously used to interpret results for electron beam irradiation in air of FEP and PFA relative to PTFE. In the more amorphous FEP and PFA, radical fragments have greater mobility to diffusion away following bond scission, while, in the highly crystalline PTFE, there is limited mobility resulting in the dominance of radical recombination reactions producing more chain branching and cross-linking [62, 63].

5. Conclusion

Vacuum UV (VUV) photo-oxidation of FEP and PFA was studied downstream from Ar microwave plasma. The modified surfaces showed: (1) an improvement in wettability as observed by water contact angle measurements; (2) surface roughening; (3) defluorination of the surface; and (4) incorporation of oxygen as CF-O-CF_2, CF_2-O-CF_2 and CF-O-CF_3 for FEP and CF-O-CF_2, CF_2-O-CF_2 and CF-O-C_nF_{2n+1} moieties for PFA which contributed to the interfacial adhesion of sputter-coated copper. With long treatment times, cohesive failure occurred within the modified FEP and PFA and not at the Cu-FEP or Cu-PFA interface.

6. Future work

In future work, nitrogen could be substituted for oxygen, in order to study the photo-nitrogenation of fluoropolymers. Incorporating nitrogen into the Teflon® surfaces should promote better adhesion than oxygen. The depth of fluoropolymer after cohesive failure, may also be investigated by studying argon ion etching in situ with XPS.

REFERENCES

1. E. T. Kang and Y. Zhang, *Adv. Mater.* **12**, 1481 (2000).
2. R. R. Rye, A. J. Howard and A. J. Ricco, *Thin Solid Films* **262**, 73 (1995).
3. R. R. Rye, *J. Polym. Sci. Polym. Phys.* **B32**, 1777 (1994).
4. J. Marchesi, K. Ha and A. Garton, *J. Adhesion* **36**, 55 (1991).
5. S. Latsch, H. Hiraoka and J. Bargon, *Mater. Res. Symp. Proc.* **385**, 239 (1995).
6. N. Inagaki, K. Narushima and T. Yamamoto, *J. Appl. Polm. Sci.* **85**, 1087 (2002).
7 G. H. Yang, E. T. Kang and K. G. Neoh, *IEEE Trans. on Adv. Packaging* **25**, 365 (2002).
8. Z. J. Yu, E. T. Kang and K. G. Neoh, *Langmuir* **18**, 10221 (2002).
9. M-K. Shi, B. Lamontagne, A. Selmani and L. Martinu, *J. Vac. Sci. Technol.* **A12**, 44 (1994).
10 N. Inagaki, *Macromol. Symp.* **159**, 151 (2000).
11. N. Inagaki, S. Tasaka and Y. W. Park, *J. Adhesion Sci. Technol.* **12**, 1105 (1998).
12 Y. W. Park, S. Tasaka and N. Inagaki, *J. Appl. Polym. Sci.* **83**, 1258 (2002).
13. J. E. Klemberg-Sapieha, M. K. Shi, L. Martinu and M. R. Wertheimer, **275**, Suppl., 10th Int. Colloquium on Plasma Processes, p.100 (1995).
14. M. K. Shi, A. Selmani, L. Martinu, E. Sacher, M. R. Wertheimer and A. Yelon, in: Polymer Surface Modification: Relevance to Adhesion, K. L. Mittal (Ed.), p. 73, VSP, Utrecht (1995).
15. J. M. Park, L. J. Matienzo and D. F. Spencer, *J. Adhesion Sci. Technol.* **5**, 153 (1991).
16. S. Zheng, A. Entenberg, G. A.Takacs, F. D. Egitto and L. J. Matienzo, *J. Adhesion Sci. Technol.* **17**, 1801 (2003).
17. H. Desai, L. Xiaolu, L., A. Entenberg, B. Kahn, F. D. Egitto, L. J. Matienzo, T. Debies and G. A. Takacs, in: Polymer Surface Modification: Relevance to Adhesion, Vol. **3**, K. L. Mittal (Ed.), pp 139-157, VSP, Utrecht (2004).
18. L. J. Matienzo, J. A. Zimmerman and F. D. Egitto, *J. Vac. Sci. Technol.* **A12**, 2662 (1994).
19. U. Sener, A. Entenberg, B. Kahn, F. D. Egitto, L. J. Matienzo, T. Debies and G. A. Takacs, in: Proc. 3rd International Symp. on Polyimides and Other High Temperature Polymers, K. L. Mittal (Ed.), Orlando, FL, Dec. 17-19 (2003).
20. F. D. Egitto, L. J. Matienzo, K. J. Blackwell and A. R. Knoll, *J. Adhesion Sci. Technol.* **8**, 411 (1994).
21. G. Rozovskis, J. Vinkevicius and J. Jaciauskiene, *J. Adhesion Sci. Technol.* **10**, 399 (1996).
22. V. Vukanovic, F. D. Egitto, F. Emmi, L. J. Matienzo, E. Matuszak and G. A. Takacs, Proc. 8th International Symp. on Plasma Chemistry, pp.933-938, Tokyo, Japan (1987).
23. V. Vukanovic, G. A. Takacs, E. A. Matuszak, F. D. Egitto, F. Emmi and R. S. Horwath, *J. Vac. Sci. Technol.* ***B6***, 66 (1988).
24. V. Mugica, J. P. Kusior, E. Matuszak, R. Clark, G. A. Takacs, V. Vukanovic, F. D. Egitto, F. Emmi and L. J. Matienzo, Proc. 9th International Symp. on Plasma Chemistry, pp.997-1002, Pugnochiuso, Italy (1989).
25. K. Lu, D. Harding, R. Clark, V. Vukanovic, F. D. Egitto, F. Emmi, L. Matienzo and G. A. Takacs, Proc. 11th International Symp. on Plasma Chemistry, Vol. 3, pp.933-938, Loughborough, England (1993).

26. L. J. Matienzo, F. Emmi, F. D. Egitto, D. C. Van Hart, V. Vukanovic and G. A. Takacs, *J. Vac. Sci. Technol.* **A6**, 950 (1988).
27. J. P. Badey, E. Urbaczewski-Espunche, Y. Jugnet, D. Sage, T. M. Duc and B. Chabert, *Polymer* **35,** 2472 (1994).
28. J. P. Lens, B. Spaay, J. G. A. Terlingen, G. H. M. Engbers and J. Feijen, *Plasmas and Polymers* **4,** 159 (1999).
29. J. A. R. Samson, Techniques of Vacuum Ultraviolet Spectroscopy, John Wiley & Sons New York (1967).
30. R. E. Huffman, J. C. Larrabee and Y. Tanaka, *Appl. Opt.* **4**, 1581 (1965).
31. J. B. Ma, J. Dagon, W. VanDerveer, A. Entenberg, V. Lindberg, M. Anschel, D. Y. Shih and P. Lauro, *J. Adhesion Sci. Technol.* **9**, 487 (1995).
32 www.dupont.com/Teflon/films/h-55007-2.pdf
33. M. Van Eesbeek, F. Levadou, V. E. Skurat, Y. I. Dorofeev, V. N. Vasilets and E. A. Barbashev, Eur. Space Agency ESA SP **368**, 165 (1994).
34. K. Seki, H. Tanaka, T. Ohta, Y. Aoki, A. Imanura, H. Fujmoto, H. Yamamoto and H. Inokuchi, *Physica Scripta* **41**, 167 (1990).
35. T. L. Cottrell, The Strengths of Chemical Bonds, 2nd ed., Butterworths, Washington, DC (1958).
36. W. A. Sheppard and C. M. Sharts, Organic Fluorine Chemistry, W.A. Benjamin, New York (1969).
37. The C-O bond energy in PFA was estimated from: (1) the bond energy in F_3C-OF using the heats of formation for CF_3 (-112.4 kcal/mol), OF (25.999 kcal/mol) and CF_3OF (-182.8 kcal/mol) [NIST Chemistry WebBook, NIST Standard Reference Database, No. 69, March (2003)] and (2) an evaluation of a wide variety of bond energy terms [G. Leroy, M. Sana, C. Wilante and M.-J. van Zieleghem, *J. Molecular Structure* **247**, 199 (1991)].
38. F. D. Egitto and L. J. Matienzo, *Polym. Degrad. Stabil.* **30**, 293 (1990).
39. J. X. Chen, D. Tracy, S. Zheng, L. Xiaolu, S. Brown, W. VanDerveer, A. Entenberg, V. Vukanovic, G. A. Takacs, F. D. Egitto, L. J. Matienzo and F. Emmi, *Polym. Degrad. Stab.* **79**, 399 (2003)
40. V. E. Skurat, E. A. Barbashev, I. A. Budashov, Y. I. Dorofeev, A. P. Nikiforov, A. I. Ternovoy, M. Van Eesbeck and F. Levadov, *Eur. Space Agency ESA SP* **399**, 267 (1997).
41. E. Grossman, Y. Noter and Y. Lifshitz, *Eur. Space Agency ESA SP* **399**, 217 (1997).
42. M. Kakehata, E. Hashimoto, F. Kannari and M.Obara, *Proc. Int. Conf. Lasers,* pp. 457-461, STS Press, McLean, VA. (1991).
43. C. L. Bungay, T. E. Tiwald, M. J. Devries, B. J. Dworak and J. A. Woollam, *Polym. Eng. Sci.* **40**, 300 (2000).
44. D. Riedel and M. C. Castex, *Appl. Phys.* **A69**, 375 (1999).
45. J. G. Calvert and J. N. Pitts, Jr., Photochemistry, John Wiley & Sons, New York (1966).
46. H. Okabe, Photochemistry of Small Molecules, John Wiley & Sons, New York (1978).
47. K. Watanabe and F. F. Marmo, *J. Chem. Phys.* **25**, 965 (1956).
48. K. K. De Groh and D. C. Smith, *Eur. Space Agency ESA SP* **399**, 255 (1997).

49. M. R. Adams and A. Garton, *Adv. Chem. Series ACS* **249**, 139 (1996).
50. A. E. Stiegman, D. E. Brinza, E. G. Laue, M. S. Anderson and R. H. Liang, *J. Spacecraft Rockets* **29**, 150 (1992).
51. F. A. Rasoul, D. J. Hill, G. A. George and J. H. O'Donnell, *Polym. Adv. Technol.* **9**, 24 (1998).
52. M. A. Golub, E. S. Lopata and L. S. Finney, *Langmuir* **10**, 3629 (1994).
53. Y. Momose, Y. Tamura, M. Ogino and S. Okazaki, *J. Vac. Sci. Technol.* **A10**, 229 (1992).
54. V. N. Vasilets, I. Hirata, H. Iwata and Y. Ikada, *J. Polym. Sci. A: Polym. Chem.* **36**, 2215 (1998).
55. S. R. Cain, F. D. Egitto and F. Emmi, *J. Vac. Sci. Technol.* **A5**, 1578 (1987).
56. C-A. Chang, Y-K. Kim and S. S. Lee, in: Metallized Plastics: Fundamentals and Applications, K. L. Mittal (Ed.) pp. 345- 354, Marcel Dekker, New York, (1998).
57. S. Wu, E. T. Kang and K. G. Neoh, *J. Adhesion Sci. Technol.* **14**, 1451 (2000).
58. H. Schonhorn and R. H. Hansen, *J. Appl. Polym. Sci.* **11**, 1461 (1967).
59. L. J. Matienzo, K. J. Blackwell, F. D. Egitto and A. R. Knoll, U. S. Patent No. 6,284,329 (2001).
60. G. M. Sessler, J. E. West, F. W. Ryan and H. Schonhorn, *J. Appl. Polym. Sci.* **17**, 3199 (1973).
61. V. N. Vasilets, K. Nakamura, Y. Uyama, S. Ogata and Y. Ikada, *Polymer* **39**, 2875 (1997).
62. T. R. Dargaville, D. J. T. Hill and A. K. Whittaker, *Radiat. Phys. Chem.* **62**, 25 (2001).
63 . K. Lunkwitz, U. Lappan and U. Scheler, *J. Fluorine Chem.* **125**, 863 (2004).